TOPICS IN THE THEORY OF HIGH-TEMPERATURE SUPERCONDUCTORS

BY

DANIEL EDWARD SHEEHY

B.A., The Johns Hopkins University, 1995
M.S., University of Illinois at Urbana-Champaign, 1998

THESIS

Submitted in partial fulfillment of the requirements
for the degree of Doctor of Philosophy in Physics
in the Graduate College of the
University of Illinois at Urbana-Champaign, 2001

Urbana, Illinois

TOPICS IN THE THEORY OF HIGH-TEMPERATURE SUPERCONDUCTORS

Daniel Edward Sheehy, Ph.D.
Department of Physics
University of Illinois at Urbana-Champaign, 2001
Prof. Paul M. Goldbart, Advisor

One important clue to understanding the origin of superconductivity in the high-temperature cuprate superconductors lies in the intriguing properties of the global phase diagram of the cuprate materials. In particular, strongly underdoped cuprates exhibit antiferromagnetic order, whereas moderately underdoped cuprate superconductors exhibit a pseudogap in the excitation spectrum above the superconducting transition temperature. It is likely that an understanding of the relationship between antiferromagnetism and superconductivity as well as an understanding of the nature of the pseudogap will be essential to the development of a theory for the cuprate superconductors.

In this Thesis we propose experimental tests aimed at assessing the validity of two particular scenarios for the cuprate superconductors. The first scenario which we examine is the phase-fluctuation model of the pseudogap phenomena, which posits that the pseudogap is due to the existence of local phase-incoherent superconducting correlations. We propose and theoretically explore experiments designed to directly probe these correlations.

The second scenario which we examine is the SO(5) theory of superconductivity, which attempts to unify the antiferromagnetic and superconducting regions of the phase diagram. We propose and theoretically explore experiments designed to test the SO(5) scenario.

Acknowledgements

I would like to acknowledge the extraordinary impact my advisor, Prof. Paul Goldbart, has had on my development as a scientist. He has been an enthusiastic and patient advisor, and sets a high standard for clarity in thought.

I would also like to acknowledge many seminal discussions with İnanç Adagideli. He has been an extremely creative and inspiring collaborator.

In addition I would also like to acknowledge Jörg Schmalian and Ali Yazdani for fruitful collaborations and discussions.

There are many other physicists to whom I am grateful for useful discussions; in particular I must acknowledge the help of Erich Mueller, Alexander Shnirman, Yuli Lyanda-Geller and Erik Draeger.

I would also like to thank my family for their support during my time in graduate school.

The work presented in this thesis was supported by the U.S. Department of Energy, Division of Materials Sciences under Award No. DEFG02-96ER45439, through the Materials Research Laboratory at the University of Illinois at Urbana-Champaign.

Contents

List of Figures

Chapter 1

Introduction

1.1 The high-temperature superconductors

The startling phenomenon of high-temperature superconductivity in the cuprates was discovered by Bednorz and Müller in 1986 [1]. Since then, several families of cuprate materials have been discovered that exhibit superconductivity; among these are $YBa_2Cu_3O_{6+\delta}$, $YBa_2Cu_4O_8$, $Bi_2Sr_2CaCu_2O_8$ and $La_{2-x}Sr_xCu_2O_4$. Although the cuprates are rather complicated structurally and chemically, they have many features in common, suggesting the promise of universality despite the current lack of a complete understanding of their electronic properties. In this Thesis we shall be concerned with models of the cuprates that focus on gross features of their electronic behavior, i.e., models that attempt to address at least some of these universal properties. In particular, we shall examine models that attempt to explain the basic structure of the cuprate phase diagram as well as the peculiar (non-metallic) behavior of the normal state of the cuprates. The purpose of the present Chapter is to give a broad overview of some universal features of the cuprates, as well as to discuss certain models that attempt to explain such features.

In Fig. 1.1 we show the generic phase diagram of the cuprates, which depicts the state of the cuprate as a function of doping and temperature. The cuprate materials are anisotropic crystals consisting of repeated layers (either one, two or three, depending on the system) of copper-oxygen (CuO_2) planes. It is currently believed that superconductivity essentially arises in these planes. At low temperatures and low doping, the cuprates are antiferromagnetic insulators (AF). Doping the cuprates amounts to adding charge carriers to the CuO_2 planes, which causes the antiferromagnetic order to be destroyed (i.e. the transition temperature T_{N} for the establishment of antiferromagnetic order goes to zero). As further charge carriers are added (i.e. at higher doping), the cuprates become superconductors (SC), with a superconducting transition temperature T_{c}. For a given material of the cuprate family, the material having the highest value of T_{c} is referred to as being "optimally doped"; materials with a lower (higher) density of dopants are referred to as being "underdoped" ("overdoped").

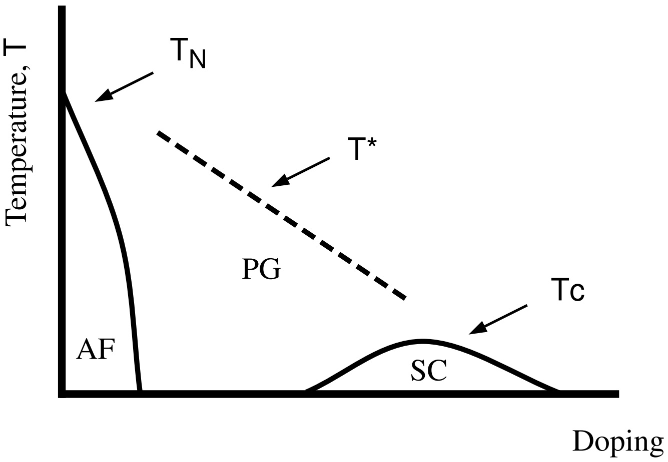

Figure 1.1: Schematic phase diagram of the high-temperature superconductors, showing the antiferromagnetic (AF) and superconducting (SC) phases as well as the pseudogap regime (PG). The temperature T^* denotes the crossover temperature below which the PG behavior sets in, T_{c} denotes the superconducting transition temperature, and T_{N} denotes the antiferromagnetic transition temperature.

At present, there is no widespread consensus regarding the mechanism for superconductivity in the cuprates; in particular, the BCS theory of superconductivity [2] (which describes the properties of conventional superconductors so well) does *not* apply to these materials. Despite this, there are certain general features of superconductors which are shared by the cuprates. Superconductivity arises from the binding of electrons into Cooper pairs. In particular, it is the coherence in phase of the Cooper-pair wave functions that leads to the infinite conductivity and the expulsion of magnetic fields. The extent to which a coherent condensate of Cooper pairs has been established can be regarded as being an order parameter for superconductivity, which we shall represent by the complex number $\Delta = |\Delta| \mathrm{e}^{i\phi}$. (We shall also refer to Δ as the pair potential.) In a conventional superconductor, the pairing of electrons is isotropic on the Fermi surface, so that Δ is independent of the orientation of the momentum space wavevector. An important distinction between the cuprates and the conventional superconductors lies in the fact that, in the cuprates, the variation of $\Delta(\mathbf{k})$ as a function of $\mathbf{k}$ on the Fermi surface has so-called d-wave symmetry [3] (i.e. $\Delta(\mathbf{k}) \propto k_x^2 - k_y^2$, where k_x and k_y are the $x-$ and $y-$components of the momentum $\mathbf{k}$). In Fig. 1.2, we sketch the basic features of a two-dimensional Fermi surface with a d-wave pair potential. One obvious consequence of a pair potential having such a form is that Δ vanishes at certain momenta (i.e. "nodes"), leading to the presence of low-energy excitations. As we shall see, the fact that $\Delta(\mathbf{k})$ changes sign on the Fermi surface also has important consequences for quasiparticle scattering. Before discussing this, however, we turn to the pseudogap regime of the cuprates.

1.2 The pseudogap regime of the cuprates

Having discussed some general properties of the cuprates, we now turn to one particular region of the cuprate phase diagram, namely the so-called "pseudogap" regime. As shown in Fig. 1.1, the pseudogap region of the phase diagram occurs for underdoped cuprates for temperatures T satisfying $T_{\mathrm{c}} < T < T^{*}$. The terminology "pseudogap"

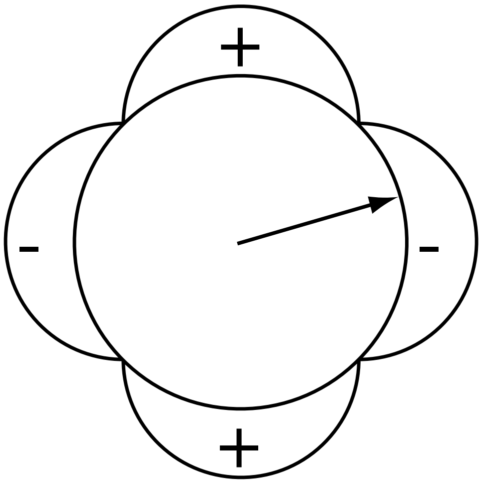

Figure 1.2: Schematic picture of the (almost everywhere) gapped Fermi surface in a d-wave superconductor, exhibiting the magnitude and sign of the d-wave order parameter. The arrow represents a general state on the Fermi surface.

refers to the apparent gap in the quasiparticle excitation spectrum for materials in this region of the phase diagram. Although the pseudogap first manifested itself in NMR experiments probing the spin-lattice relaxation rate [4], one of the the most direct probes of the pseudogap has turned out to be scanning tunneling spectroscopy (STS) [5, 6]. STS experiments consist of bringing a metal tip close to the surface of the sample and applying a bias voltage $\hbar\omega/e$ between the tip and the sample. Electrons then tunnel through the region (i.e. vacuum or perhaps an oxide layer) between the tip and sample surface. The conductance measured in such an experiment yields the single-particle density of states $N(\omega)$ of the sample.

In a conventional superconductor, the presence of superconducting correlations influences the low-ω structure of behavior of $N(\omega)$ in the following manner: At low energies, there are no single particle excitations (all electrons having formed Cooper pairs), so that $N(\omega) = 0$ for $\hbar\omega < \Delta$. Thus, to excite an electron a Cooper pair must be destroyed. In a conventional superconductor, $\Delta \to 0$ as $T \to T_{\rm c}$ from below so that the excitation gap closes. By contrast, in the underdoped cuprate superconductors the single particle excitation gap appears to *not* close at $T_{\rm c}$, and instead appears to persist up to remarkably high temperatures [5, 6]. In addition, angle-resolved photoemission (ARPES) experiments [7] have shown that the angular dependence of the pseudogap appears to have a d-wave form, indicating that the pseudogap evolves continuously into the superconducting gap.

Although there have been several scenarios [8] attempting to describe the pseudogap phenomena, here we shall focus on two particular ones. The first scenario invokes the notion that the pseudogap is due to the presence of local Cooper pairing that leads to a gap in the excitation spectrum but lacks the long-range coherence in phase necessary for actual superconductivity. There are several scenarios that contain the notion that the pseudogap is due to such pairing correlations [11, 14]; in particular, we focus on the phase-fluctuation picture [14–17].

The second scenario of the pseudogap phenomena that we address in this Thesis is the SO(5) theory [9]. The SO(5) theory attempts to unify antiferromagnetic and superconducting regimes of the cuprate phase diagram by combining the antiferromagnetic and superconducting order parameters into a five dimensional order parameter. Within this theory, the establishment of a nonzero mean magnitude of this order parameter occurs at the pseudogap onset temperature T^*.

In the next section, we discuss the phase-fluctuations scenario of the pseudogap, and then in Sec. 1.4 we turn to the the SO(5) approach.

1.3 The phase-fluctuation scenario of the pseudogap regime

According to the phase-fluctuation [14–16] scenario of the pseudogap regime, the destruction of superconducting order at T_c arises from fluctuations of the phase ϕ of the superconducting order parameter. Such fluctuations may be thought of as occurring from the proliferation of superconducting vortices (i.e. points in the sample at which $\boldsymbol{\nabla} \times \boldsymbol{\nabla}\phi \neq \mathbf{0}$). Thus, although pairing correlations are present (and are responsible for the gap in the excitation spectrum) long-range coherence in ϕ is absent. The phase-fluctuation scenario was first proposed by Emery and Kivelson [14]; they argued that the low superfluid density and quasi-two-dimensional nature of the cuprate superconductors makes them especially susceptible to phase fluctuations. This scenario (and scenarios involving pairing correlations above T_c in general) appear natural, given that, as we discussed in Sec. 1.2, the superconducting gap appears to evolve continuously into the pseudogap. Additional evidence for the phase-fluctuation scenario comes from the Nernst effect data of Xu et al. [18], who find evidence of vortex-like excitations above T_c in La_{2-x} Sr_x Cu O_4.

An important test for the phase fluctuation scenario would be furnished by experiments that directly probe the spatially and temporally transient pairing correlations present in such a phase. Experimental evidence of precisely this nature has been furnished by the experiments of Corson et al. [19] on the high-frequency electrical conductivity of $Bi_2Sr_2CaCu_2O_{8+\delta}$. According to their analysis (which is based on the theoretical analysis of the two-dimensional XY model of Ambegaokar et al. [20]), the vortex excitations which preclude the existence of long-range superconducting order have a certain diffusion time. By measuring the AC conductivity at frequencies that are fast compared to this time (so that vortices are unable to "screen" a phase twist), Corson et al. are able to probe the microscopic pairing correlations purported to exist in the pseudogap regime.

One way of envisioning the electronic properties of the pseudogap regime, then, is in terms of a system that possesses local superconducting correlations, the phase of which fluctuates due to the presence and motion of vortices. Our main goal in Chapters 2 and 3 of this Thesis shall be to propose and examine experimental probes designed to access these local superconducting correlations. However, we first consider the SO(5) theory of high-temperature superconductivity and antiferromagnetism.

1.4 The SO(5) theory of the high-T_c superconductors

The SO(5) theory of high-temperature superconductivity, introduced by Zhang, [9] amounts to an attempt to understand the global structure of the cuprate phase diagram. At low temperatures, and as a function of doping, the cuprates pass from an antiferromagnetic state to a superconducting state; thus, a minimal model describing such materials should exhibit both of the aforementioned types of order. The SO(5) model does this by considering the symmetries associated with the antiferromagnetic and superconducting sectors. Although the SO(5) model has been related, theoretically, to more microscopic models of the cuprates (such as the t-J model [9]), we can understand the basic origin of the SO(5) model via the following considerations: The low-energy behavior of an antiferromagnet may be understood qualitatively in terms of the broken symmetry associated with the establishment of antiferromagnetic order. The order parameter for an antiferromagnet, the Néel vector $\mathbf{N}$, may point in any direction in real space; the manifold of symmetry-related orientations of $\mathbf{N}$ is therefore the two-dimensional surface of the three-dimensional unit sphere S_2. The low-energy spin-wave excitations of an antiferromagnet correspond to local spatial and temporal variations of $\mathbf{N}$ (i.e. the Goldstone modes).

Similarly, one can study the broken symmetry associated with the establishment of long-range superconducting order. As noted in Sec. 1.1, the order parameter for superconductivity Δ consists of an amplitude $|\Delta|$ and a phase ϕ. Whereas $|\Delta|$ is more or less fixed in the superconducting state, ϕ is arbitrary. The manifold of symmetry-related orientations of Δ is thus represented by the unit circle in the complex plane. Although this is a gauge symmetry and, hence, conceptually different from the broken symmetry state of the antiferromagnet, we will ignore this distinction in motivating the SO(5) theory.

The SO(5) theory attempts to unify the three-dimensional symmetry sector (i.e. S_2) associated with antiferromagnetic order with the two-dimensional symmetry sector associated with the superconducting order (i.e. the circle of phases S_1) by combining the antiferromagnetic and superconducting order parameters into a five-dimensional unit-vector order parameter $\mathbf{n}$ (called the "superspin"). The components of $\mathbf{n}$ together determine the local state of the system with regard to the establishment of antiferromagnetic and superconducting order. Thus, one possible assignment would be that n^1, n^2 and n^3 together specify $\mathbf{N}$ (e.g. $N_x = n^1$, $N_y = n^2$, $N_z = n^3$), and the components n^4 and n^5 together specify the amplitude and phase of Δ (e.g. $\mathrm{Re}[\Delta] = n^4$, $\mathrm{Im}[\Delta] = n^5$). As noted above, the ground-state configuration of the cuprates includes both antiferromagnetic and superconducting regimes; thus the SO(5) model is constructed to have a doping-dependent anisotropy which causes the ground-state orientation of $\mathbf{n}$ to lie in either the antiferromagnetic subspace or the superconducting subspace. To be concrete, we consider a particular form for the SO(5) free-energy density:

$$f = \frac{\rho}{2} \sum_{a=1}^{5} \partial_\mu n^a \, \partial_\mu n^a - \frac{g}{2} \sum_{a=1}^{3} (n^a)^2 \,, \tag{1.1}$$

where the (real-space) subscript μ runs from 1 to 3 (or x, y, z), with repeated indices being summed over. The first term in Eq. (1.1) amounts to a nonlinear sigma model, and favors uniform configurations of the unit vector $\mathbf{n}$; the corresponding stiffness parameter is given by ρ. The (doping-dependent) anisotropy parameter g determines, via the second term in Eq. (1.1), whether the stable uniform ground state is antiferromagnetic ($g > 0$) or superconducting ($g < 0$).

Within the SO(5) theory, then, the finite magnitude of $\mathbf{n}$ corresponds to the fact that, at high temperatures (presumably at the pseudogap temperature scale) electrons pair into singlets that could coalesce into either antiferromagnetic or superconducting order. At low temperatures, $\mathbf{n}$ selects a ground-state orientation in the SC or AF phase, depending on the value of the anisotropy parameter g. However, fluctuations of the superspin in the superconducting phase may lead to the presence of antiferromagnetic order in an ostensibly superconducting material. Conversely, one expects that, within the S0(5) theory, excitations of the superspin in the antiferromagnetic regime may create local domains of superconductivity. In this Thesis we shall study each of the aforementioned cases. The main goals of Chapters 4 and 5 is to propose experiments that test the SO(5) theory via precisely these effects.

1.5 Overview

This Thesis is organized as follows. In Chapter 2, we show how the intimate relationship between d-wave pairing correlations and low-energy electronic states near impurities implies that such low-energy states provide a potentially useful probe of the putative pairing correlations in the pseudogap regime of the cuprates. In Chapter 3, we consider another potential probe of pairing correlations in the pseudogap regime of the cuprates, namely Andreev interferometry. In Chapter 4, we turn to the SO(5) model of high-temperature superconductivity, and show how the conductance of thin superconducting wires should exhibit a signature of the SO(5) theory. This signature is associated with the fact that, within the SO(5) model, the dissipation processes in a thin wire involve the creation of local antiferromagnetic order. In Chapter 5, we examine another feature of the SO(5) theory, namely that in the antiferromagnetic phase certain topological excitations lead to the presence of local superconducting correlations.

The research presented in Chapter 2 was done in collaboration with İnanç Adagideli, Paul M. Goldbart and Ali Yazdani. The research presented in Chapter 3 was done in collaboration with Goldbart, Jörg Schmalian and Yazdani. The research presented in Chapters 4 and 5 was done in collaboration with Goldbart.

Chapter 2

Density of states as a probe of superconducting pairing correlations in the pseudogap regime of the cuprates

2.1 Introduction

Among the challenges presented by the high-temperature superconductors, one of the most persistent concerns the anomalous properties of the *normal* state of these materials. In particular, the suppression of single-particle spectral weight around the Fermi energy [6, 21, 22] for temperatures above the superconducting transition temperature T_c of the underdoped cuprates indicates that the electronic behavior of these materials deviates substantially from that of conventional superconductors. There have been several theoretical scenarios proposed to explain this so-called pseudogap behavior [8]. In the present work, we shall be concerned with a particular one of these, viz., the phase-fluctuation scenario [14–17]. According to this scenario (which we have already discussed in Sec. 1.3), superconducting correlations in the form of Cooper pairing are presumed to exist (and to be responsible for the loss of single-particle spectral weight) for temperatures T below the pseudogap onset temperature T^{*}. However, in the intermediate temperature range (i.e. $T_{\mathrm{c}} < T < T^{*}$) the long-range spatial and temporal coherence in phase of the Cooper-pair wave functions (occurring for $T < T_{\mathrm{c}}$) is presumed to be present only up to intermediate length scales, having been disrupted on longer length scales by the presence and motion of vortex excitations. In other words, although long-range phase coherence is absent in it, the pseudogap regime is quantitatively distinguished from the conventional non-superconducting state by the presence of substantial, residual, local d-wave pairing correlations.

Several recent experimental investigations support the notion of the phase fluctuation scenario as the origin of pseudogap phenomenology, including Refs. [18, 19]. Further steps towards an understanding the nature of the pseudogap regime would be furnished by experimental probes that are targeted towards the question of the existence of the putative local superconducting correlations [23–26]. Such probes would have the potential to discriminate between scenarios based on pairing correlations and those in which the pseudogap is due to some other mode of electronic ordering [8]. The purpose of the present work is to identify one such probe: scanning tunneling spectroscopy (STS) measurements of the single-particle spectral function near extended impurities in the pseudogap regime [27].

Before explaining the nature of this probe, let us pause to recall one of its essential ingredients. It has long been recognized [28–30] that the scattering of quasiparticles between states corresponding to differing signs of the d-wave pair-potential leads to the existence of low-energy states [31]. Such scattering, and hence low-energy state-formation, occurs, e.g., at suitably oriented surfaces in the cuprates, leading to the observed zero-bias anomaly in the tunneling conductance [33]. In the setting of impurity (rather than boundary) scattering in d-wave superconductors, low-energy states, which in this case are localized near the impurities, have been observed in STS experiments [34, 35], and have been discussed theoretically for the case of point-like [32] and extended [36, 37] impurities. We remind the reader that these states co-exist with the continuum of low-energy quasiparticle states associated with the nodes at which the d-wave pair-potential vanishes. Distinguishing between impurity states and nodal states is straightforward because the former give a peaked contribution to the spectral function whereas the contribution from the latter vanishes linearly at zero energy. (A clear example of this is furnished by the data reported in Ref. [34].)

Returning to our main task, viz., probing the pseudogap regime for pairing correlations, we now state the central idea on which the present work is based. Let us suppose that the pseudogap state is indeed distinguished by the presence of local (but not long range) d-wave pairing correlations. The lack of long-range phase coherence in such a state complicates the experimental observation of the more conventional signatures of superconducting correlations (such as the Meissner effect). However, the low-energy quasiparticle states occurring near extended impurities are *localized* in space, i.e., their existence only relies on the presence of local d-wave pairing correlations. In consequence, these states should be only weakly affected by the destruction of long-range superconducting order that occurs at T_c, and hence should "survive" the transition into the pseudogap state. Thus, if STS experiments were to reveal a sharp feature in the single-particle spectral function at low voltage bias, this would be evidence for the presence of local d-wave pairing correlations. And if such experiments were able to characterize the temperature- and doping-dependence of the width of this spectral feature, this would provide a characterization of the nature of these finite-range spatial and temporal correlations.

Why are we focusing on the case of (non-magnetic) *extended* impurities as a probe of the pseudogap regime? The main reason underlying this choice is as follows. In the setting of extended impurities (as well as boundaries) in the superconducting state, it has been shown that the existence of low-energy quasiparticle states is a direct consequence of the d-wave nature (or, more precisely, the sign-changing nature) of the pair-potential [36]. Continuing this reasoning to the case of extended impurities in the pseudogap regime, there the existence of low-energy states strongly depends on the presence of superconducting correlations of d-wave type.

We note that Kruis et al. [40] have studied the density of states near a *point-like* impurity in the context of a simple phenomenological picture of the pseudogap regime. In this picture, the physics of the pseudogap regime is incorporated through the hypothesis that, in the absence of the impurity, the single-particle density of states vanishes linearly at the Fermi energy. At present, the extent to which an approach based on this picture can yield information about pairing correlations in the pseudogap regime is not clear.

This Chapter is organized as follows. In Sec. 2.2 we provide a framework for discussing the influence of local d-wave pairing correlations on quasiparticle states near extended impurities [41], focusing on the single-particle spectral function. As we shall see, our expression for this spectral function will take the form of a density of states (determined at a fixed, locally phase-randomized d-wave pair-potential) averaged over the fluctuations of the phase field. In Sec. 2.3 we develop a semiclassical scheme for computing this density of states at fixed pair-potential in which we treat the long-wavelength pair-potential phase variations via perturbation theory. This scheme allows us to focus on the contribution to the density of states at low energies, which involves states arising from changes in sign (as the momentum is varied) of the local pair-potential. At this point we will have obtained an expression for the spectral function which consists of a sum of terms each associated with one classical scattering trajectory that passes through the vicinity of the impurity potential. In Sec. 2.4.1 we perform the average over the configurations of the fluctuating pair-potential arrived at via local randomizations of the phase, under the assumption that the distribution of phase-field configurations is Gaussian. We make an approximation to the resulting expression for the spectral function that is valid for the case of phase correlations persisting beyond the Cooper-pair size, finally arriving at an expression for the spectral function near an extended impurity that consists of a Gaussian peak the linewidth of which is proportional to the typical gradient of the phase of the pair-potential. In this section we also compute the linewidth of the spectral function in the pseudogap regime, doing so by assuming that the phase fluctuations are governed by the BKT theory of the two-dimensional XY-model. Finally, in Sec. 2.5 we make a numerical estimate of the linewidth by invoking the results of recent high-frequency conductivity data [19], and provide some concluding remarks.

The research presented in this Chapter has been reported in Ref. [42].

2.2 Model of cuprates with an extended impurity

In the present section we formulate the task of obtaining the single-particle spectral function in settings of systems of fermions interacting via some fermion-fermion coupling and also interacting with an external single-fermion potential (which could, e.g., represent an impurity potential). As our aim is to address the phase-fluctuation picture of the pseudogap regime of the cuprates, we envision following the standard field-theoretic route (see, e.g., Ref. [43] or Appendix A) of exchanging the fermion-fermion coupling for a suitable collective quantum field Δ. Thus we arrive at the following formula for the one-fermion Green function $\mathcal{G}(x,x')$[c.f. Eq. (A.10)]:

$$\mathcal{G}(x,x') = \frac{\displaystyle\int D\Delta^\dagger D\Delta\, \mathrm{e}^{-S[\Delta]}\, G(x,x';\Delta)}{\displaystyle\int D\Delta^\dagger D\Delta\, \mathrm{e}^{-S[\Delta]}}, \tag{2.1}$$

$$\begin{pmatrix} \partial_\tau + \hat{h} & \hat{\Delta} \\ \hat{\Delta}^\dagger & \partial_\tau - \hat{h} \end{pmatrix} G(x,x';\Delta) = -\delta(x-x'), \tag{2.2}$$

i.e., a Bogoliubov–de Gennes Green function for pair-potential Δ, suitably averaged over Δ, the action for which is $S[\Delta]$. Here, $x \equiv (\mathbf{r}, \tau)$ where $\mathbf{r}$ and τ are respectively the spatial position (in the two-dimensional CuO_2 plane) and the Matsubara time. Furthermore, $\hat{h} \equiv -\nabla^2 - k_{\mathrm{F}}^2 + V(\mathbf{r})$, in which k_{F}^2 is the chemical potential [i.e. k_{F} ($\equiv 2\pi/\lambda_{\mathrm{F}}$) is the Fermi wave vector], V is the single-particle potential, and we have adopted units in which $\hbar^2/2m = 1$, m being the (effective) mass of the electrons and holes. The operator $\hat{\Delta}$ is the pair-potential (integral) operator; how it acts is specified by the nonlocal kernel $\Delta(x, x')$ via $[\hat{\Delta}v](x) = \int dx' \Delta(x, x')\, v(x')$.

Our primary interest is in spectral function $\rho(E)$ in the pseudogap regime as well as the superconducting-to-pseudogap transition regime. This quantity can be obtained in the usual way from $\mathcal{G}(x, x')$ as follows:

$$\rho(E) \equiv -\pi^{-1} \mathrm{Im}\, \mathrm{Tr} \int d^2 r\, \mathcal{G}(\mathbf{r}, \mathbf{r}; \omega_n)|_{i\omega_n \to E + i\delta}, \tag{2.3}$$

$$\mathcal{G}(\mathbf{r}, \mathbf{r}'; \omega_n) \equiv \int_0^\beta d\tau\, \mathrm{e}^{i\omega_n \tau} \mathcal{G}(\mathbf{r}, \mathbf{r}'; \tau, 0), \tag{2.4}$$

where Tr denotes a trace only in the 2×2 particle-hole space, $\beta \equiv 1/T$ (i.e., we have chosen units in which Boltzmann's constant $k_{\mathrm{B}} = 1$) and the $\omega_n \equiv (2n+1)\pi T$ (with n integral) are fermionic Matsubara frequencies, and $\delta = 0+$. We shall assume that the temperature is sufficiently high to validate the neglect of nonzero Matsubara-frequency modes of Δ, which amounts to treating Δ as a classical (i.e. nonquantal) statistical field. Under this static condition, in which the fermion dynamics takes place in the presence of an unchanging Δ field, the spectral function $\rho(E)$ may be expressed in the form

$$\rho(E) = \langle \rho(E; \Delta) \rangle, \tag{2.5}$$

$$\rho(E; \Delta) = \sum\nolimits_n \delta(E - E_n), \tag{2.6}$$

where $\{E_n\}$ is the collection of energy eigenvalues of the following Bogoliubov–

de Gennes eigenproblem in the presence of a generic classical configuration of Δ:

$$\begin{pmatrix} \hat{h} & \hat{\Delta} \\ \hat{\Delta}^\dagger & -\hat{h} \end{pmatrix} \begin{pmatrix} u \\ v \end{pmatrix} = E \begin{pmatrix} u \\ v \end{pmatrix}. \tag{2.7}$$

The notation $\langle \cdots \rangle$ denotes the aforementioned static average over Δ, i.e.,

$$\langle \mathcal{O} \rangle \equiv \frac{\int D\Delta^\dagger D\Delta \, \mathrm{e}^{-S[\Delta]} \, \mathcal{O}}{\int D\Delta^\dagger D\Delta \, \mathrm{e}^{-S[\Delta]}}. \tag{2.8}$$

(We do not specifically indicate that this functional average is only over static configurations of Δ.) Thus we have expressed the single-particle spectral function $\rho(E)$ in terms of a suitably averaged density of states $\rho(E;\Delta)$ for a corresponding Bogoliubov–de Gennes eigenproblem.

Before proceeding with the analysis of the eigenproblem given in Eq. (2.7), we address the issue of the form of the pairing fluctuations that contribute dominantly to the average in Eq. (2.5). This amounts to a statement about the physical picture of the pseudogap regime that we are concerned with. Now, as discussed shortly before Eq. (2.5), we are considering only *static* configurations of Δ, and therefore we shall henceforth simplify the notation by writing the pair-potential kernel $\Delta(x, x')$ as $\Delta(x, x') = \Delta(\mathbf{r}, \mathbf{r}')$. In addition, it is convenient to transform $\Delta(\mathbf{r}, \mathbf{r}')$ to relative and center-of-mass coordinates, $\boldsymbol{\rho}$ and $\mathbf{R}$:

$$\bar{\Delta}(\boldsymbol{\rho}, \mathbf{R}) \equiv \Delta(\mathbf{r}, \mathbf{r}'), \quad \boldsymbol{\rho} \equiv \mathbf{r} - \mathbf{r}', \quad 2\mathbf{R} \equiv \mathbf{r} + \mathbf{r}'. \tag{2.9}$$

It is then convenient to introduce the Fourier transform of $\bar{\Delta}$ with respect to the relative coordinate $\boldsymbol{\rho}$, viz., $\bar{\Delta}(\mathbf{k}, \mathbf{R})$:

$$\bar{\Delta}(\mathbf{k}, \mathbf{R}) \equiv \int d^2\rho \, \mathrm{e}^{-i\mathbf{k}\cdot\boldsymbol{\rho}} \bar{\Delta}(\boldsymbol{\rho}, \mathbf{R}), \tag{2.10}$$

thus obtaining a pair-potential at center-of-mass position $\mathbf{R}$ and relative momentum $\mathbf{k}$.

As mentioned in Sec. 2.1, the scenario for the pseudogap regime with which we are concerned is based on the dominance of configurations of $\bar{\Delta}(\mathbf{k}, \mathbf{R})$ of the form

$$\bar{\Delta}(\mathbf{k}, \mathbf{R}) = \bar{\Delta}_0(\mathbf{k}, \mathbf{R}) \, \mathrm{e}^{i\phi(\mathbf{R})}. \tag{2.11}$$

Here, the nonfluctuating factor $\bar{\Delta}_0(\mathbf{k}, \mathbf{R})$ is taken to have d-wave form (and can therefore be taken to be real) [44]. The fluctuating factor $\exp i\phi(\mathbf{R})$ varies slowly with $\mathbf{R}$. By assuming this form for $\bar{\Delta}(\mathbf{k}, \mathbf{R})$ we are adopting the physical picture of the state as being one in which there is no long-range superconducting order, but there are local d-wave superconducting correlations, embodied in $\bar{\Delta}_0(\mathbf{k}, \mathbf{R})$ [45].

In the following section, we obtain $\rho(E; \Delta)$ by making use of an elaboration of Andreev's semiclassical approach [46] to the Bogoliubov–de Gennes eigenproblem. This elaboration is appropriate for the setting at hand, viz., one in which there is a strong single-particle potential. This scheme was used in Ref. [36] in order to address the low-energy density of states near an extended impurity in a d-wave superconducting state having a negligibly fluctuating, well-formed condensate. In contrast, our focus here is on situations in which the fluctuations in the *amplitude* of Δ are small, but the *phase* of Δ is strongly fluctuating. Thus, although there is local pairing the system does does not exhibit long-range order.

2.3 Semiclassical approach

In Sec. 2.2 we showed how the single-particle spectral function $\rho(E)$ can be expressed as a density of states $\rho(E; \Delta)$ for the Bogoliubov–de Gennes eigenproblem at arbitrary pair-potential Δ, averaged over Δ with a suitable weight, provided Δ can be treated in the static approximation. To make progress with this Bogoliubov–de Gennes eigenproblem we invoke, in the present section, a semiclassical approximation under which Eq. (2.7) reduces to a family of one-dimensional eigenproblems labeled by the classical scattering trajectories of a particle in the presence of the single-particle potential $V(\mathbf{r})$. This approximation scheme, which was developed in Ref. [36], is valid provided that $k_{\mathrm{F}}^2 \gg \{\Delta_0, E\}$ for physically relevant configurations of Δ (where Δ_0 is the magnitude of Δ), and provided that $V(\mathbf{r})$ and relevant configurations of Δ vary slowly on the scale of the Fermi wavelength $\lambda_{\rm F}$.

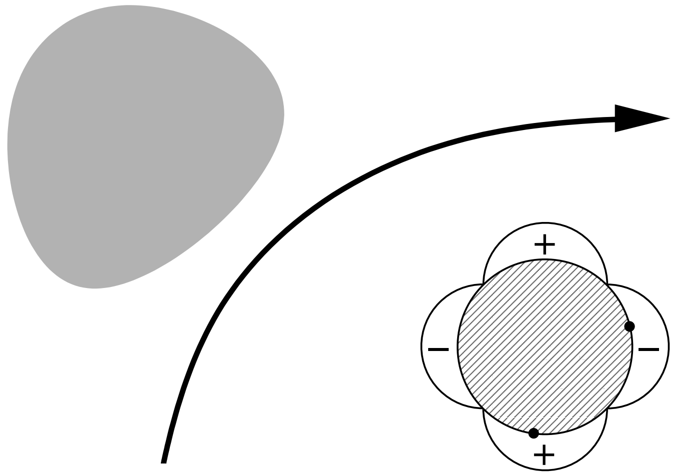

Figure 2.1: Schematic illustration of a classical trajectory for a quasiparticle scattering from an extended impurity. Also shown is a depiction of the background d-wave pair-potential; dots indicate incoming and outgoing quasiparticle momenta.

We now turn to the family of one-dimensional eigenproblems arising in our semi-classical scheme. Following Ref. [36](see also Appendix B), it is straightforward to determine that the emerging trajectory-dependent eigenproblem has the form

$$\hat{H}\begin{pmatrix}\bar{u}\\ \bar{v}\end{pmatrix} = E\begin{pmatrix}\bar{u}\\ \bar{v}\end{pmatrix}, \tag{2.12}$$

$$\hat{H} \equiv \begin{pmatrix} -2ik_{\rm F}\,\partial_s & \Delta_0(s)\exp i\phi(s) \\ \Delta_0(s)\exp -i\phi(s) & 2ik_{\rm F}\,\partial_s \end{pmatrix}, \tag{2.13}$$

$$\Delta_0(s) \simeq \bar{\Delta}_0(k_{\rm F}\partial_s\mathbf{x}_{\rm c}(s), \mathbf{x}_{\rm c}(s)). \tag{2.14}$$

Here, $\phi(s) \simeq \phi(\mathbf{x}_{\rm c}(s))$, and the parameter s measures the position along a particular classical trajectory $\mathbf{x}_{\rm c}(s)$, the latter obeying the Newton equation

$$k_{\rm F}^2\,\partial_s^2\mathbf{x}_{\rm c}(s) = -\boldsymbol{\nabla}V(\mathbf{x}_{\rm c}(s)). \tag{2.15}$$

In Fig. 2.1 we depict a typical classical trajectory in the vicinity of an impurity potential. Each such classical trajectory (and associated eigenproblem) is labeled by an impact parameter b and an incoming momentum direction $\mathbf{n}$.

Our next task is to obtain the low-energy eigenvalues associated with Eq. (2.12) for the case of a d-wave pair-potential subject to generic spatial phase variations, i.e., Eq. (2.11). To do this, we perform a local unitary transformation of $\hat{H}$, i.e., $\hat{H} \to U\,\hat{H}\,U^{\dagger}$, where

$$U(s) \equiv \begin{pmatrix} \mathrm{e}^{-i\phi(s)/2} & 0 \\ 0 & \mathrm{e}^{i\phi(s)/2} \end{pmatrix}, \tag{2.16}$$

and thus our eigenproblem acquires the form

$$(\hat{H}_0 + \hat{H}_1) \begin{pmatrix} \bar{u} \\ \bar{v} \end{pmatrix} = E \begin{pmatrix} \bar{u} \\ \bar{v} \end{pmatrix}, \tag{2.17}$$

$$\hat{H}_0(s) \equiv \begin{pmatrix} -2ik_{\mathrm{F}}\,\partial_s & \Delta_0(s) \\ \Delta_0(s) & 2ik_{\mathrm{F}}\,\partial_s \end{pmatrix}, \tag{2.18}$$

$$\hat{H}_1(s) \equiv \begin{pmatrix} k_{\mathrm{F}}\,\partial_s\phi & 0 \\ 0 & k_{\mathrm{F}}\,\partial_s\phi \end{pmatrix}. \tag{2.19}$$

The Hamiltonian for this eigenproblem now consists of a term arising from the underlying d-wave pair-potential (i.e. $\hat{H}_0$) as well as a term that contains all the phase-variation information (i.e. $\hat{H}_1$). Our strategy is to treat $\hat{H}_1$ within perturbation theory, the starting point for which is the identification of the eigenstates of $\hat{H}_0$. As our purpose is to address low-energy states, it is adequate for us to focus on the *zero-energy* eigenstate of $\hat{H}_0$, if any there be. As we shall discuss below, such states are guaranteed to arise for certain classical trajectories $\mathbf{x}_{\mathrm{c}}(s)$ [36, 38]. The condition for the existence of such a state is determined by the asymptotic properties of $\Delta_0(s)$: If $\Delta_0(s)$ changes sign an odd number of times along an entire trajectory then the Hamiltonian $\hat{H}_0$ associated with that trajectory has precisely one zero-energy eigenstate. Said more formally, if $\Delta_{\pm} \equiv \lim_{s\to\pm\infty} \Delta_0(s)$ then the condition for the existence of the zero-energy state is that $\Delta_+\Delta_- < 0$. The explicit form of this eigenstate is

$$\psi_\pm(s) \;=\; \frac{1}{\sqrt{2}}\begin{pmatrix}\varphi_\pm(s)\\ \pm i\varphi_\pm(s)\end{pmatrix}, \tag{2.20}$$

$$\varphi_\pm(s) \;\equiv\; \alpha_\pm \exp \pm (2k_{\mathrm{F}})^{-1}\int^{s} ds'\,\Delta_0(s')\,, \tag{2.21}$$

where ψ_+ corresponds to the case $\Delta_+ < 0$ (so that $\Delta_- > 0$) and ψ_- corresponds to the case $\Delta_+ > 0$ (so that $\Delta_- < 0$). The prefactors $\alpha_\pm$ are normalization factors, chosen so that $\int_{-\infty}^{\infty}\varphi_\pm(s)^2 ds = 1$.

Let us emphasize some of the important features of these zero-energy states that hold provided the scatterer creates only trajectories with at most a single sign change in the pair-potential [47]. First, the presence or absence of these states depends *only* on the properties of the d-wave pair-potential far from any impurity, and is insensitive to any amplitude variations of the d-wave pair-potential that might occur in the vicinity of this impurity. Second, the wavefunctions $\psi_\pm(s)$ exhibit exponential decay away from the impurity with a decay constant of order $k_{\mathrm{F}}/|\Delta_\pm|$, which is proportional to the BCS correlation length. As this length-scale is known to be short in the cuprates, these states are indeed an extremely *local* probe of local superconducting correlations.

In the absence of phase fluctuations (i.e. in the pure d-wave superconductor), these zero-energy eigenstates lead to a sharp peak in the density of states at low-energies [36]. To access the impact of order-parameter phase variations on this peak, we include the effect of $\hat{H}_1$ on the zero-energy state $\psi_\pm(s)$ within quantum-mechanical perturbation theory. Thus, the shift in energy of the previously zero-energy eigenstate associated with a particular trajectory $\mathbf{x}_{\mathrm{c}}(s)$ (parameterized by $\mathbf{n}$ and b) is given by

$$\epsilon(\mathbf{n}, b) \;\equiv\; \int ds\,\psi_\pm^\dagger(s)\,\hat{H}_1(s)\,\psi_\pm(s), \tag{2.22}$$

$$\;=\; k_{\mathrm{F}}\int ds\,\partial_s\,\phi(s)\,\varphi_\pm(s)^2, \tag{2.23}$$

where we have used Eq. (2.20) to get from Eq. (2.22) to Eq. (2.23). The spectral function at fixed pair-potential $\rho(E, \Delta)$ consists of contributions from all trajectories $\mathbf{x}_c(s)$. As we are restricting our attention to low energies, it is sufficient to consider only trajectories for which $\Delta_+\Delta_- < 0$ (i.e., those for which $\hat{H}_0$ has a zero-energy state). The contribution to the low-energy spectral function at constant pair-potential due to the perturbed zero-energy states is given by

$$\rho(E, \Delta) \simeq k_{\mathrm{F}} \int \frac{d\mathbf{n}}{2\pi} \int db\, \delta\big(E - \epsilon(\mathbf{n}, b)\big) \times (1 - \operatorname{sgn} \Delta_+ \operatorname{sgn} \Delta_-)\,, \tag{2.24}$$

where the factor $(1 - \operatorname{sgn} \Delta_+ \operatorname{sgn} \Delta_-)$ ensures that only trajectories that satisfy the condition $\Delta_+\Delta_- < 0$ (i.e. exhibit an asymptotic sign change in $\Delta_0(s)$) contribute.

It is important to emphasize that Eq. (2.24) only includes the contribution from the perturbed zero-energy states, and that there will be additional, smaller contributions to the density of states at low energies. Sources of these include remnants of the near-nodal quasiparticles states that exist in pure, d-wave superconductors at arbitrarily low energies.

2.4 Averaging over phase fluctuations

In Sec. 2.3 we obtained an expression for the Bogoliubov–de Gennes density of states $\rho(E, \Delta)$ in the presence of an extended impurity for the case of a pair-potential with local d-wave character and specific realization of the spatially varying phase $\phi(\mathbf{r})$; see Eq. (2.24). In the present section, we calculate the spectral function $\rho(E)$ in the pseudogap regime by averaging $\rho(E, \Delta)$ over suitable configurations of $\phi(\mathbf{r})$, i.e., by inserting Eq. (2.24) into Eq. (2.5). We remind the reader that our scheme for computing $\rho(E)$ applies to settings in which the temperature is high enough that we may treat the phase fluctuations classically, as discussed after Eq. (2.4).

2.4.1 Gaussian model for phase fluctuations

In order to evaluate the average over configurations of the pair-potential in Eq. (2.5) explicitly, we need a model for the weight of the various configurations. For the sake of simplicity, we choose the phase-field configurations to have a (zero mean) Gaussian distribution characterized by the correlator $\langle \nabla_\alpha \phi(\mathbf{r}) \nabla_\beta \phi(\mathbf{r}') \rangle$. In terms of this correlator, it is straightforward to show that the spectral function $\rho(E)$ is a superposition of Gaussian distributions, one associated with each classical trajectory on which Δ_0 changes sign:

$$\begin{aligned} \rho(E) &\simeq k_{\mathrm{F}} \int \frac{d\mathbf{n}}{2\pi} \int db \, \frac{\exp\left(-E^2/2\langle \epsilon(\mathbf{n},b)^2\rangle\right)}{\sqrt{2\pi\langle \epsilon(\mathbf{n},b)^2\rangle}} \\ &\qquad \times \left(1 - \operatorname{sgn}\Delta_+ \operatorname{sgn}\Delta_-\right), \end{aligned} \tag{2.25}$$

$$\langle \epsilon(\mathbf{n},b)^2\rangle \equiv k_{\mathrm{F}}^2 \int ds \int ds' \, \varphi_\pm^2(s)\, \varphi_\pm^2(s')\, \langle \dot{\phi}(s)\, \dot{\phi}(s')\rangle. \tag{2.26}$$

Here, $\dot{\phi}(s) \equiv \partial_s \phi(s)$, and the width $\langle \epsilon(\mathbf{n},b)^2\rangle$ of each Gaussian contribution is sensitive to the degree to which local superconducting correlations have been disrupted, as can be seen by the presence of the phase-phase correlator $\langle \dot{\phi}(s)\, \dot{\phi}(s')\rangle$ in Eq. (2.26). Our next task, then, is to evaluate the integrals over the parameters s and s' in Eq. (2.26) in order to determine the width $\langle \epsilon(\mathbf{n},b)^2\rangle$ associated with each trajectory $(\mathbf{n},b)$. In the next section, we carry out this evaluation within an approximation that is valid for the case of long-wavelength phase fluctuations.

2.4.2 Approximate evaluation of trajectory integrals

In Sec. 2.4.1, we obtained the expression (2.25) for the spectral function $\rho(E)$ near an extended impurity in the pseudogap regime. In the present section, we make an approximation to our expression for $\rho(E)$ that makes use of the *local* nature of the low-energy states, as well as the long-wavelength nature of the pair-potential phase variations (appropriate for $T \approx T_{\mathrm{c}}$). By *local* we mean that the wave functions $\varphi_\pm(s)$ exhibit exponential decay over a length-scale $\xi \sim k_{\mathrm{F}}/|\Delta_\pm|$, i.e., the BCS correlation length; this can be seen by examining Eq. (2.21); see [48]. In the cuprate superconductors, this length-scale is expected to be much shorter than the length-scale ξ_ϕ for typical pair-potential phase variations (i.e. the inter-vortex spacing). Thus one has a separation of lengthscales: $\xi_\phi > \xi$. (Such a separation is a natural ingredient of the phase-fluctuation picture of the pseudogap regime because for inter-vortex spacings on the order of ξ the conventional meaning of local Cooper pairs appears to break down.)

To make the approximation to our expression for $\rho(E)$, consider the integrations over the trajectory parameters s and s' in Eq. (2.26). Now, the correlation function $\langle\dot{\phi}(s)\,\dot{\phi}(s')\rangle$ varies appreciably only over lengthscales on the order of ξ_ϕ or longer, whereas the wavefunctions $\varphi_\pm$ decay exponentially, as mentioned, on the lengthscale ξ. Hence, one can make an asymptotic approximation to the s and s' integrations which amounts to pulling the correlator out of the integrals. Thus, owing to the normalization of $\varphi_\pm$, we have

$$\langle\epsilon^2\rangle \simeq k_{\mathrm{F}}^2\langle\dot{\phi}(0)\,\dot{\phi}(0)\rangle, \tag{2.27}$$

independent of $\mathbf{n}$ and b.

Next, we turn to the interpretation of the quantity $\langle\dot{\phi}(0)\,\dot{\phi}(0)\rangle$. The derivative of the phase along a particular trajectory is given by

$$\dot{\phi}(s) = \dot{\mathbf{x}}_{\mathrm{c}}(s)\cdot\boldsymbol{\nabla}\phi(\mathbf{x})\big|_{\mathbf{x}=\mathbf{x}_{\mathrm{c}}(s)}, \tag{2.28}$$

By inserting Eq. (2.28) into Eq. (2.27), we see that the correlator of interest is $\langle\nabla_\alpha\phi(\mathbf{r})\nabla_\beta\phi(\mathbf{r})\rangle$ which, by spatial isotropy, has the form $\delta_{\alpha\beta}\,\langle|\boldsymbol{\nabla}\phi(\mathbf{r})|^2\rangle/2$. According to the phase-fluctuation scenario, vortex excitations are the dominant mechanism for generating phase gradients .

How does this information about the phase correlations translate into information about the spectral function? By noting that trajectories $\mathbf{x}_{\mathrm{c}}(s)$ involving sign-changes in the d-wave pair-potential obey $|\dot{\mathbf{x}}_{\rm c}| \sim 1$ and using the aforementioned phase-gradient correlator, we arrive at the width

$$\langle \epsilon^2 \rangle \sim k_{\rm F}^2 \langle |\boldsymbol{\nabla}\phi(\mathbf{r})|^2 \rangle / 2 \tag{2.29}$$

and, hence, our final expression for the spectral function $\rho(E)$:

$$\begin{aligned} \rho(E) \;\; &\simeq \;\; \frac{\exp\left(-E^2/2\langle\epsilon^2\rangle\right)}{\sqrt{2\pi\langle\epsilon^2\rangle}} \\ &\quad \times k_{\rm F} \int \frac{d\mathbf{n}}{2\pi} \int db \, \left(1 - \operatorname{sgn}\Delta_+ \operatorname{sgn}\Delta_-\right). \end{aligned} \tag{2.30}$$

The first factor is a Gaussian in the energy E with a linewidth $\langle\epsilon^2\rangle^{1/2}$ associated with the r.m.s. fluctuations in the phase gradient. The second factor (i.e. the integral over the impact parameter b and the incoming momentum direction $\mathbf{n}$) determines the scale for $\rho(E)$, essentially by counting the number of sign-changing trajectories, and is expected to be only weakly temperature dependent. In the next section, we compute the linewidth within a Berezinskiĭ-Kosterlitz-Thouless-like (BKT) model of phase fluctuations near $T_{\rm c}$.

2.4.3 Linewidth near the superconducting phase boundary

To make further progress, we now attempt to calculate the spectral function linewidth due to the phase fluctuations accompanying the destruction of superconducting order in the neighborhood of $T_{\rm c}$. We shall do this by choosing a particular weight for the phase fluctuations, viz., that associated with the two-dimensional XY-model [49–51]. Our analysis is reminiscent of that due to Franz and Millis [15] who addressed the bulk single-particle spectral function in the pseudogap regime. In the present context, this analysis is provided solely for illustrative purposes, and is only meant only to provide a rough estimate of the linewidth.

Let us consider the XY-model action,

$$S[\Delta] = \frac{K}{2} \int d^2 r \, |\boldsymbol{\nabla}\phi|^2, \tag{2.31}$$

where $K \equiv \rho_s(T)/T$ in which $\rho_s(T)$ is the temperature-dependent superfluid density [52]. Note that we are not suggesting that the true critical fluctuations of the cuprate superconductors necessarily lie in the universality class of the two-dimensional XY-model, but simply that the intermediate lengthscale fluctuations proposed as leading to pseudogap phenomena may adequately be modeled by Eq. (2.31). The form for $\langle|\boldsymbol{\nabla}\phi(\mathbf{r})|^2\rangle$ for the XY-model may be calculated following the Debye-Hückel-type analysis of Halperin and Nelson [54], which gives

$$\langle|\boldsymbol{\nabla}\phi(\mathbf{r})|^2\rangle \simeq \frac{2}{\pi\xi_\phi^2 K^*}\ln\Lambda\xi_\phi, \tag{2.32}$$

in which K^* is the short lengthscale stiffness (obtained using the Kosterlitz renormalization group equations), Λ is a short-distance cutoff, and ξ_ϕ is a lengthscale characterizing the typical inter-vortex spacing. The principal temperature dependence in Eq. (2.32) arises via ξ_ϕ: near T_{BKT} [i.e. the transition temperature of the model (2.31), which is expected to lie not far below T_{c}] ξ_ϕ is proportional to $\exp\sqrt{\Theta/(T-T_{\mathrm{BKT}})}$, where Θ is a constant of order unity (which we do not attempt to calculate in detail).

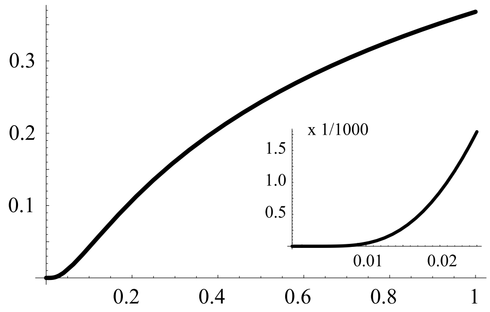

Figure 2.2: Spectral linewidth versus $(T - T_{\mathrm{BKT}})/\Theta$. Inset: Immediate vicinity of the transition.

The proliferation of unbound vortex excitations upon warming through the BKT transition is reflected by this strong diminution of ξ_ϕ and causes a concomitant dramatic increase in the linewidth of the spectral function:

$$\langle\epsilon^2\rangle^{1/2} \propto \exp\left(-\sqrt{\Theta/(T-T_{\mathrm{BKT}})}\right), \tag{2.33}$$

which we depict in Fig. 2.2. Observation of a fluctuation-broadened peak in the spectral function, e.g., via STS measurements, would provide striking evidence in support of the phase-fluctuation scenario. Moreover, the temperature dependence of the linewidth would, e.g., provide access to the details of the vortex-unbinding transition.

2.5 Numerical estimate of the linewidth; concluding remarks

In the previous section we saw how one could estimate the temperature dependence of the linewidth of the spectral function near the superconducting transition temperature T_{c}. In the present section we make a rough numerical estimate of this linewidth at one particular temperature in the pseudogap regime by appealing to the data obtained in the high-frequency conductivity experiments of Corson et al. [19] on $\mathrm{Bi_2Sr_2CaCu_2O_{8+\delta}}$. We shall be specifically concerned with the interpretation of these data inasmuch as they provide access to the characteristic vortex density.

Until now we have been working with a system of units in which $\hbar^2/2m = 1$. Restoring conventional units in Eq. (2.29) gives for the linewidth

$$\langle \epsilon^2 \rangle^{1/2} \sim \frac{\hbar^2}{2m} k_{\mathrm{F}} \langle |\boldsymbol{\nabla}\phi(\mathbf{r})|^2/2 \rangle^{1/2}. \tag{2.34}$$

To estimate this width, we turn to the Corson et al. experiments and its analysis by Corson et al., which is based on the notion that, at sufficiently high frequencies, the conductivity probes short-lengthscale pairing correlations, and leads to an estimate for the characteristic density of free vortices n_{f}. Assuming that it is vortex excitations that lead to phase fluctuations, one expects that, up to a constant of order unity, $\langle |\boldsymbol{\nabla}\phi(\mathbf{r})|^2 \rangle \simeq n_{\mathrm{f}}$.

Now, Corson et al. obtain values of n_f that are on the order of $0.003\, a_{\mathrm{vc}}$ (for $T \sim 75K$), where a_{vc} is the area of the core of a vortex. If we take the vortex core to be a disk of radius $\xi \simeq 1\,\mathrm{nm}$, this leads to the value $n_{\mathrm{f}} \sim 10^3\,\mu\mathrm{m}^{-2}$. Then, using the order-of-magnitude estimate $k_{\mathrm{F}} \simeq 1\,\mathrm{nm}^{-1}$, Eq. (2.34) gives $\langle\epsilon^2\rangle^{1/2} \simeq 9\,\mathrm{meV}$.

The value of this estimate is that it shows that, for at least one cuprate material, there is a temperature at which the free-vortex density is small enough that phase fluctuations only weakly perturb the energies of the quasiparticle states. Hence, the linewidth arising from perturbed zero-energy states can be rather smaller than the scale of the superconducting energy gap (and hence small enough to justify the our picture of perturbed zero-modes) but be large enough to be resolvable in STS measurements, such as those of Yazdani et al. [34]. Larger densities of free vortices, and hence large linewidths, would result from working at higher temperatures. Moreover, near T_{c} the vortex density is expected to show a very strong dependence on temperature, which should confer a strong temperature dependence on the linewidth. Of course, if conducted at the temperature of the Corson et al. experiments, thermal broadening would complicate the task of accessing the intrinsic linewidth (i.e. the linewidth due to phase fluctuations); recall that $10\,\mathrm{K}$ is equivalent to $1\,\mathrm{meV}$. Thus, one should consider performing experiments on materials having a lower T_{c}, so that the pseudogap regime can be explored at temperatures at which thermal broadening is less significant. Thus, it is at least conceivable that STS experiments near extended scatterers could provide a sharp test of the phase fluctuation scenario for the pseudogap regime.

Chapter 3

Andreev interferometry as a probe of superconducting phase correlations in the pseudogap regime of the cuprates

3.1 Introduction

A range of experimental investigations have indicated that underdoped high-temperature superconductors (HTSCs) exhibit intriguing properties at temperatures *above* the superconducting transition temperature T_c. Most notably, these materials show a strong suppression in the single-particle electronic spectral weight at low energies, even at temperatures far above T_c [6, 21, 22], a property referred to as the *pseudogap*. A number of scenarios have been proposed to account for this loss of spectral weight [11, 12, 14, 55–59], several of which invoke the notion that remnants of superconducting correlations remain in the non-superconducting state [11, 14, 57–59], i.e., that pairing is established locally but that it lacks the long-range coherence in *phase* necessary for true superconductivity.

To make progress with understanding the nature of the pseudogap regime, having experimental access to the *spatial structure* of the correlated electronic state is likely to be of considerable value [60]. In this Chapter we identify one possible scheme, involving low-voltage mesoscopic conductance measurements, for probing this structure experimentally, and describe this scheme within the context of a simple theoretical model.

The basic idea is this. Let us adopt as a working hypothesis the picture of the pseudogap regime in which superconductivity is established locally, but in which the presence and motion of vortices in the superconducting order parameter cause the phase of the superconducting order parameter to be randomized beyond certain correlation length- and time-scales [62]. The effects of such phase fluctuations on the single-particle properties of underdoped cuprates have been explored in Refs. [15, 16]. In Chapter 2 we studied the effect of phase fluctuations on the single particle properties near extended impurities. Now, the low-voltage conductance of a normal–to–superconducting junction includes contributions associated with the Andreev reflection of quasiparticles from the superconducting condensate [63]. What about the low-voltage conductance of a normal–to–pseudogap junction? Given the picture of the pseudogap regime outlined above, and assuming that tunneling through the junction occurs on a time-scale faster than the time-scale for vortex rearrangement, we anticipate that there will be contributions to the conductance due to the Andreev reflection of quasiparticles from the *local* superconductivity. However, owing to the phase sensitivity of the Andreev reflection process [67], any spatial variation in the phase of the superconducting order parameter over the junction would tend to cause (diffraction-like) interference of the quasiparticle/hole waves that have been Andreev reflected from the junction, and thereby diminish the associated contribution to the conductance.

Now suppose that the normal contact in a normal–to–pseudogap junction has a characteristic linear dimension L. If L is smaller than the characteristic phase-phase correlation (i.e. inter-vortex) length ξ_ϕ (e.g. the smaller contact in Fig. 3.1) then, at any instant, rather little phase variation would be expected over the contact and the Andreev contribution to the conductance should be barely diminished. However, if L is substantially larger than ξ_ϕ (e.g. the larger contact in Fig. 3.1) then considerable phase variation is expected over the contact, and the Andreev contribution to the conductance is likely to be strongly suppressed. Measurements made using a range of mesoscopic contact sizes [68] thus have the capability of providing a direct probe of the spatial correlations of the phase of the superconducting order parameter at various temperatures within the pseudogap regime.

Let us emphasize that the concept of Andreev interferometry is by no means new; indeed, several groups have considered this concept both theoretically [69] and experimentally [70]. However, to the best of our knowledge this interferometry has primarily been considered in contexts in which reflection is from a truly superconducting region (rather than from a pseudogap region), and in settings in which the phase has an average value that varies in a relatively simple way in space (such as on either side of a Josephson junction). Here, we are considering a setting in which the interferometry is being used as a probe of the superconducting fluctuations. It should be mentioned that in recent work Choi et al. [23] considered the issue of whether or not Andreev reflections would survive at temperatures above T_c. This work involves applying the BTK technique [66] to the physical picture of the pseudogap regime explored, e.g., in Refs. [15, 16]. It amounts to a computation of the conductance of a normal–to–superconductor interface for a d-wave superconductor in a uniform supercurrent-carrying state, this conductance then being averaged over a Gaussian distribution of uniform supercurrents (in order to model the pseudogap state). This yields a conductance dependent upon the statistical distribution of local values of the supercurrent arising from varying vortex locations. In contrast, the present work fo-

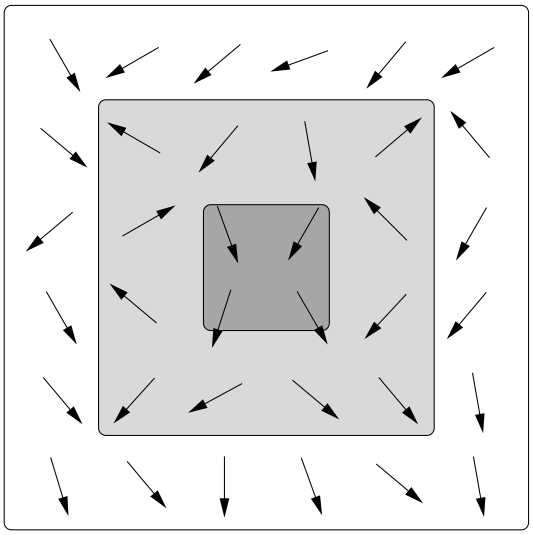

Figure 3.1: Schematic depiction of an instantaneous configuration of the superconducting phase in the pseudogap state (arrows). The two shades of gray indicate two possible (normal-state) contact areas on the pseudogap (i.e. white) substrate. Whereas the smaller (i.e. darker) contact abuts a region of nearly uniform phase, the larger (i.e. lighter) contact exhibits regions of considerably differing phase.

cuses on the spatial correlations of the phase in the pseudogap regime and, specifically, how such correlations may be accessed experimentally.

The research presented in this Chapter has been reported in Ref. [25].

3.2 Tunneling current for a normal–to–pseudogap junction

We now illustrate the ideas of Sec. 3.1 by computing the conductance of a normal–to–pseudogap junction within the tunneling formalism, and show how this conductance depends on the pseudogap phase-phase correlation function. To this end, we adopt as the tunneling Hamiltonian H_{T} [71] between a normal state (N) and a pseudogap state (P):

$$H_{\mathrm{T}} \equiv \sum_{\sigma=\pm} \int_{\mathrm{P}} d^3r \int_{\mathrm{N}} d^3s \left(t_{\mathbf{r},\mathbf{s}}\, d^{\dagger}_{\mathbf{r},\sigma}\, c_{\mathbf{s},\sigma} + t^{*}_{\mathbf{r},\mathbf{s}}\, c^{\dagger}_{\mathbf{s},\sigma}\, d_{\mathbf{r},\sigma} \right), \tag{3.1}$$

where the position $\mathbf{s}$ lies on the normal side of the junction and the position $\mathbf{r}$ lies on the pseudogap side. The operators $c_{\mathbf{s},\sigma}$ (or $c^\dagger_{\mathbf{s},\sigma}$) and $d_{\mathbf{r},\sigma}$ (or $d^\dagger_{\mathbf{r},\sigma}$) respectively annihilate (or create) quasiparticles with spin projection σ on the normal side at $\mathbf{s}$ and on the pseudogap side at $\mathbf{r}$. We choose the interface to be in the plane $z = 0$ (where $\{x, y, z\}$ are Cartesian coordinates and $\{\mathbf{e}_x, \mathbf{e}_y, \mathbf{e}_z\}$ are the corresponding basis vectors) and, accordingly, decompose vectors such as $\mathbf{s}$ and $\mathbf{r}$ into components parallel (e.g. $\boldsymbol{\sigma}$) and perpendicular (e.g. $s_z\mathbf{e}_z$) to the interface so that $\mathbf{s} = \boldsymbol{\sigma} + s_z\mathbf{e}_z$ and $\mathbf{r} = \boldsymbol{\rho} + r_z\mathbf{e}_z$. This choice, together with the assumption that tunneling only occurs locally at the interface leads us to assert that the tunneling matrix elements $t_{\mathbf{r},\mathbf{s}}$ are given by

$$t_{\mathbf{r},\mathbf{s}} = t_0 a\, \delta^{(1)}(s_z)\, \delta^{(1)}(r_z)\, \delta^{(2)}(\boldsymbol{\sigma} - \boldsymbol{\rho}), \tag{3.2}$$

where a is a microscopic length scale characterizing the thickness of the “active” layer for tunneling of particles and t_0 is the typical energy scale for this process.

Next, we compute the current $I(V)$ as a function of the voltage V. To do this, we consider the expectation value of the tunneling current operator $[-eQ_{\mathrm{N}}, H_{\mathrm{T}}]/i\hbar$, where $-e$ is the electron charge:

$$-\frac{ie}{\hbar}\sum_{\sigma=\pm}\int_{\mathrm{P}} d^3r \int_{\mathrm{N}} d^3s \left(t_{\mathbf{r},\mathbf{s}}\, d^\dagger_{\mathbf{r},\sigma}\, c_{\mathbf{s},\sigma} - t^*_{\mathbf{r},\mathbf{s}}\, c^\dagger_{\mathbf{s},\sigma} d_{\mathbf{r},\sigma}\right), \tag{3.3}$$

with respect to the full Hamiltonian for the system, i.e., $H = H_{\mathrm{N}} + H_{\mathrm{P}} + H_{\mathrm{T}}$, where $H_{\mathrm{N/P}}$ is the Hamiltonian for the normal/pseudogap side and $-eQ_{\mathrm{N}}$ is the charge operator for the normal side. In fact, it is convenient to obtain $I(V)$ perturbatively in the tunneling amplitude $t_0 a$ by applying the Matsubara technique to the imaginary-time dependent tunneling current $\tilde{I}(\tau_1)$ [72]. The lowest-order term, which is of order $|t_0 a|^2$, represents the normal (i.e. single-particle) current. This contribution is suppressed at low voltages due to the presence of a gap at low energies on the pseudogap side. The next-order contribution to $\tilde{I}$, which is of fourth order in $t_0 a$, is given by (see Appendix C for details)

$$
\begin{aligned}
\tilde{I}(\tau_1) = -\frac{e}{\hbar}|t_0 a|^4 \sum_{\sigma_i=\pm} \int_{\mathcal{A}} \prod_{j=1}^{4} d^2\rho_j \int_0^\beta d\tau_2\, d\tau_3\, d\tau_4 \\
\times \big\langle T_\tau\, d^\dagger_{\boldsymbol{\rho}_1,\sigma_1}(\tau_1)\, d^\dagger_{\boldsymbol{\rho}_2,\sigma_2}(\tau_2)\, d_{\boldsymbol{\rho}_3,\sigma_3}(\tau_3)\, d_{\boldsymbol{\rho}_4,\sigma_4}(\tau_4)\big\rangle_{\mathrm{P}} \\
\times \big\langle T_\tau\, c_{\boldsymbol{\rho}_1,\sigma_1}(\tau_1)\, c_{\boldsymbol{\rho}_2,\sigma_2}(\tau_2)\, c^\dagger_{\boldsymbol{\rho}_3,\sigma_3}(\tau_3)\, c^\dagger_{\boldsymbol{\rho}_4,\sigma_4}(\tau_4)\big\rangle_{\mathrm{N}} \\
\times\, \mathrm{e}^{-i\omega_\delta(\tau_2+\tau_3+\tau_4)}\, \mathrm{e}^{-i\Omega(\tau_1+\tau_2-\tau_3-\tau_4)},
\end{aligned}
\tag{3.4}
$$

where $\langle\cdots\rangle_{\mathrm{P/N}}$ indicates an equilibrium expectation value with respect to $H_{\mathrm{P/N}}$, and β measures the inverse temperature. Operators such as $c_{\mathbf{r},\sigma}(\tau)$ [or $d_{\mathbf{s},\sigma}(\tau)$] are interaction-picture operators, i.e., $\mathrm{e}^{K_0\tau}c_{\mathbf{r},\sigma}\mathrm{e}^{-K_0\tau}$ (or $\mathrm{e}^{K_0\tau}d_{\mathbf{s},\sigma}\mathrm{e}^{-K_0\tau}$), where $K_0 \equiv H_{\mathrm{N}} - \mu_{\mathrm{N}}Q_{\mathrm{N}}$ (or $K_0 \equiv H_{\mathrm{P}} - \mu_{\mathrm{P}}Q_{\mathrm{P}}$). Here, μ_{N} (or μ_{P}) is the chemical potential on the normal (or pseudogap) side, and Q_{N} (or Q_{P}) is the charge operator for the normal (or pseudogap) side. The physical current $I(V)$ is given by the imaginary part of $\tilde{I}(\tau_1)$ after making the following analytical continuations: $i\omega_\delta \to i0^+$, $i\Omega \to eV$ (i.e. the voltage across the junction), and $-i\hbar\tau_1 \to t$ (i.e. the time).

To apply Eq. (3.4) to the setting at hand, namely one side of the junction being normal and the other being in the pseudogap regime, we shall need to evaluate the two two-particle Green function factors that feature in it, one for the normal side and one for the pseudogap side. For the normal side, we assume that the corresponding two-particle Green function is factorizable into two single-particle Green functions, i.e.,

$$
\begin{aligned}
&\big\langle T_\tau\, c_{\boldsymbol{\rho}_1,+}(\tau_1)\, c_{\boldsymbol{\rho}_2,-}(\tau_2)\, c^\dagger_{\boldsymbol{\rho}_3,-}(\tau_3)\, c^\dagger_{\boldsymbol{\rho}_4,+}(\tau_4)\big\rangle_{\mathrm{N}}, \\
&\quad = G^{\mathrm{N}}(\boldsymbol{\rho}_1,\boldsymbol{\rho}_4;\tau_1-\tau_4)\, G^{\mathrm{N}}(\boldsymbol{\rho}_2,\boldsymbol{\rho}_3;\tau_2-\tau_3),
\end{aligned}
\tag{3.5}
$$

where $G^{\mathrm{N}}(\boldsymbol{\rho},\boldsymbol{\rho}';\tau-\tau') \equiv \langle T_\tau\, c_{\boldsymbol{\rho},\sigma}(\tau)\, c^\dagger_{\boldsymbol{\rho}',\sigma}(\tau')\rangle$ is the single-particle Green function on the normal side. On the other hand, for the pseudogap side we adopt a model in which the pseudogap state is a superconductor that is "disordered" by a *static* pattern of vortices and characterized by a *static* phase-phase correlator. We do not require information concerning the dynamic phase-phase correlation function because we are assuming that the Andreev reflection process is rapid, compared with the time needed for vortices to substantially rearrange the phase structure. To support this assumption, let us note that the time-scale associated with Andreev reflection is of order $\tau_{\mathrm{AR}} \sim \xi_{\mathrm{a}}/v_{\mathrm{F}}$, where v_{F} is the Fermi velocity of the incoming electron and ξ_{a} is the amplitude-fluctuation correlation length (i.e. the Cooper-pair size) on the pseudogap side. Then, by using the estimates $v_{\mathrm{F}} \approx 10^7 \mathrm{cm/s}$ and $\xi_{\mathrm{a}} \approx 1\,\mathrm{nm}$ (typical for a HTSC) we find that $\tau_{\mathrm{AR}} \sim 10^{-14}\,\mathrm{s}$. The experiments of Corson et al. [19] indicate that the vortex-pattern rearrangement time corresponds to frequencies in the terahertz range (i.e. is of order $10^{-9}\,\mathrm{s}$) so that, at least as a starting point, we may neglect the dynamics of the vortices. Thus, we assume that quasiparticles incident from the normal side effectively encounter, and are Andreev reflected by, a static pair-potential that has a nonzero amplitude (except at the vortex cores, which are small) and a spatially random phase. With this in mind, we characterize the pseudogap side by the anomalous Green function

$$\begin{aligned} F^{\mathrm{P}}(\mathbf{r},\mathbf{r}';\tau,\tau') &\equiv \langle T_\tau\, d_{\mathbf{r},\downarrow}(\tau)\, d_{\mathbf{r}',\uparrow}(\tau')\rangle_{\mathrm{P}} \\ &= f_0(\mathbf{r}-\mathbf{r}';\tau-\tau')\, \mathrm{e}^{i(\phi(\mathbf{r})+\phi(\mathbf{r}'))/2}, \end{aligned} \tag{3.6}$$

where the phase $\phi(\mathbf{r})$ varies randomly in space, and the function f_0 is given by the value it takes in a conventional superconductor [73], i.e.,

$$\begin{aligned} f_0(\mathbf{r};\tau) &= \int \frac{d^3k}{(2\pi\hbar)^3}\frac{1}{\beta}\sum_{n=-\infty}^{\infty} \mathrm{e}^{i\omega_n\tau}\mathrm{e}^{i\mathbf{k}\cdot\mathbf{r}/\hbar} \\ &\qquad \times \left(\frac{\Delta_{\mathbf{k}}}{2E_{\mathbf{k}}}\right)\left(\frac{1}{i\omega_n+E_{\mathbf{k}}}-\frac{1}{i\omega_n-E_{\mathbf{k}}}\right). \end{aligned} \tag{3.7}$$

Here, $E_{\mathbf{k}}$ [$\equiv \sqrt{\xi_{\mathbf{k}}^2+\Delta_{\mathbf{k}}^2}$, with $\xi_{\mathbf{k}} \equiv (\hbar^2k^2/2m)-\mu$] is the excitation energy in the pseudogap material and $\Delta_{\mathbf{k}}$ is the gap amplitude. The Matsubara frequencies ω_n are defined to be $\omega_n = (2n+1)\pi/\beta$ for integer n. For the sake of simplicity, we now focus on the case of s-wave pairing and thus set $\Delta_{\mathbf{k}} = \Delta$ [74]. We approximate the two-particle Green function on the P side in Eq. (3.4) by making a Gorkov factorization into the anomalous Green function F^{P} and its conjugate. In principle, there will also be a contribution associated with factorization into normal Green functions. However, these contributions are suppressed at low voltages, and thus it is adequate to take for the current

$$\begin{aligned}\tilde{I}(\tau_1) \quad = \quad & -\frac{2e}{\beta}|t_0 a|^4 \int_{\mathcal{A}} \prod_{j=1}^{4} d^2\rho_j \mathrm{e}^{i(\phi(\boldsymbol{\rho}_1)+\phi(\boldsymbol{\rho}_2)-\phi(\boldsymbol{\rho}_3)-\phi(\boldsymbol{\rho}_4))/2} \\ & \times \sum_{n=-\infty}^{\infty} G^{\mathrm{N}}(\boldsymbol{\rho}_2, \boldsymbol{\rho}_3; i\omega_n + i\omega_\delta + i\Omega) \\ & \times G^{\mathrm{N}}(\boldsymbol{\rho}_1, \boldsymbol{\rho}_4; -i\omega_n - 3i\omega_\delta + i\Omega) \\ & \times f_0(\boldsymbol{\rho}_1 - \boldsymbol{\rho}_2; i\omega_n)\ f_0(\boldsymbol{\rho}_3 - \boldsymbol{\rho}_4; i\omega_n + 2i\omega_\delta), \end{aligned} \tag{3.8}$$

where the limit $\mathcal{A}$ indicates that the interface integrals are constrained to the area of the contact between the N and P regions. Equation (3.8) may be expressed diagrammatically, as shown in Fig. 3.2, where one-arrow lines denote normal Green functions, two-arrow lines denote anomalous Green functions (and the straight line denotes the interface). We see that this contribution to the current involves the correlation of an electron and a hole propagating on the normal side, mediated by the static random pair-potential on the pseudogap side of the junction.

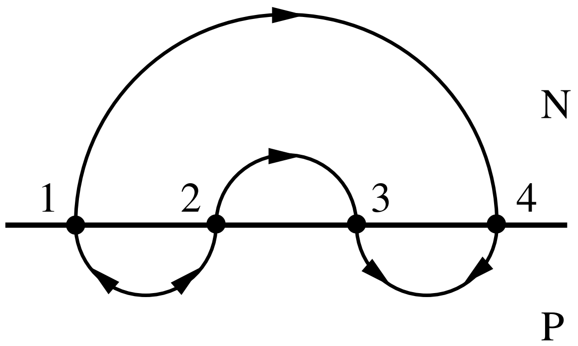

Figure 3.2: Diagram depicting the leading-order (in tunneling amplitude) phase-sensitive contribution to the current.

Equation (3.8), which represents the leading contribution due to Andreev reflection at an interface, may be considerably simplified in situations in which $\xi_{\mathrm{a}} \ll \xi_\phi$

(i.e. the phase order which we are interested in probing via Andreev reflection persists over length scales much larger than the pair size), which is not only the case for the usual NS interface setting but also for the present NP setting. To support this assertion, we obtain the ratio of these two length-scales by examining the results of the Corson et al. experiments on the high-frequency AC conductivity of $Bi_2Sr_2CaCu_2O_{8+\delta}$ [19]. According to the analysis of Corson et al., in the pseudogap state the ratio of ξ_ϕ to ξ_{a} is related to the vortex diffusion time τ via

$$\left(\frac{\xi_\phi}{\xi_{\mathrm{a}}}\right)^2 = \frac{\tau\Omega_0}{2\pi}, \tag{3.9}$$

where Ω_0 is a parameter determined by Corson et al. to be $1.14 \times 10^{14}\,\mathrm{s}^{-1}$. From Fig. (4) of Corson et al., we see that at $T = 75\,\mathrm{K}$, $\tau \sim 10^{-12}\,\mathrm{s}$, so that $\xi_\phi^2/\xi_{\mathrm{a}}^2 \sim 20$.

The significance of the separation of the length-scales ξ_{a} and ξ_ϕ in the present context follows from the fact that the function f_0 has spatial range ξ_{a}. Thus, in Eq. (3.8) the spatial integrations over the coordinates $\{\boldsymbol{\rho}_i\}_{i=1}^4$ may be simplified because f_0 varies rather more rapidly in space than do the other factors in the integrand. This allows us to make the approximation

$$\begin{aligned} f_0(\boldsymbol{\rho}, i\omega) &\approx \delta^{(2)}(\boldsymbol{\rho}) \int_{\mathcal{A}} d^2\boldsymbol{\rho}'\, f_0(\boldsymbol{\rho}', i\omega) \\ &\approx \delta^{(2)}(\boldsymbol{\rho}) \int_{-\infty}^{\infty} \frac{dk_z}{2\pi\hbar}\, \hat{f}_0(k_z\mathbf{e}_z, i\omega), \end{aligned} \tag{3.10}$$

where $\hat{f}_0$ is the (three-dimensional) Fourier transform of f_0 and k_z is the momentum component perpendicular to the interface. By using this approximation, we obtain

$$\begin{aligned} \tilde{I}(\tau_1) = -\frac{2e}{\beta}|t_0 a|^4 &\sum_{n=-\infty}^{\infty} \int_{\mathcal{A}} d^2\rho_1 \int_{\mathcal{A}} d^2\rho_2\, \mathrm{e}^{i(\phi(\boldsymbol{\rho}_1)-\phi(\boldsymbol{\rho}_2))} \\ &\times G^{\mathrm{N}}(\boldsymbol{\rho}_1, \boldsymbol{\rho}_2; i\omega_n + i\omega_\delta + i\Omega) \\ &\times G^{\mathrm{N}}(\boldsymbol{\rho}_1, \boldsymbol{\rho}_2; -i\omega_n - 3i\omega_\delta + i\Omega) \\ &\times \int \frac{dk_z}{2\pi\hbar}\, \hat{f}_0(k_z\mathbf{e}_z, i\omega_n) \int \frac{dk_z'}{2\pi\hbar}\, \hat{f}_0(k_z'\mathbf{e}_z, i\omega_n + 2i\omega_\delta). \end{aligned} \tag{3.11}$$

Having derived Eq. (3.11), an equation applicable to any given realization of the phase field $\phi(\boldsymbol{\rho})$ on the P-side of the interface, we conclude the present section by averaging this current over an as-yet-unspecified distribution of phase fields. As discussed above, the time-scale for the tunneling process is shorter than the time-scale for phase rearrangement. Thus, it is appropriate to proceed as we have, by first computing the current for a fixed realization of the phase field, and then to construct the time-averaged current, averaged over times longer than the phase rearrangement time, by averaging the current over an appropriate (in this case, equilibrium) distribution of phase fields. Denoting such averaging by $[\cdots]$, and introducing the appropriate phase-phase correlator

$$g(\boldsymbol{\rho}_1 - \boldsymbol{\rho}_2) \equiv \big[\mathrm{e}^{i\phi(\boldsymbol{\rho}_1)}\,\mathrm{e}^{-i\phi(\boldsymbol{\rho}_2)}\big], \tag{3.12}$$

we arrive at a formula for the time-averaged current $\big[\tilde{I}(\tau_1)\big]$, i.e., Eq. (3.11) but with the phase factors $\exp i\big(\phi(\boldsymbol{\rho}_1) - \phi(\boldsymbol{\rho}_2)\big)$ replaced by $g(\boldsymbol{\rho}_1 - \boldsymbol{\rho}_2)$. For convenience, we express the normal-side Green function in terms the corresponding spectral function A:

$$G^{\mathrm{N}}(\boldsymbol{\rho}_1, \boldsymbol{\rho}_2; i\omega_n) \equiv \int_{-\infty}^{\infty} \frac{d\epsilon}{2\pi} \frac{A(\boldsymbol{\rho}_1, \boldsymbol{\rho}_2; \epsilon)}{i\omega_n - \epsilon}. \tag{3.13}$$

Then we may perform the integrations over k_z and k'_z (by converting them to energy integrals), as well as the summation over Matsubara frequencies. By performing the necessary analytic continuations and taking the imaginary part, we obtain an expression for the tunneling current $I(V)$ through a mesoscopic interface between a normal metal and a material in the pseudogap state:

$$\begin{aligned} I(V) \;=\; & \frac{e}{\hbar}\frac{\pi}{8}|t_0 a|^4 \tilde{\nu}_{\mathrm{P}}^2 \int_{\mathcal{A}} d^2\rho_1 \int_{\mathcal{A}} d^2\rho_2 \; g(\boldsymbol{\rho}_1 - \boldsymbol{\rho}_2) \\ & \times \int_{-\mu}^{2eV+\mu} d\epsilon \frac{\Delta^2}{\Delta^2 - (eV-\epsilon)^2} \big\{ n(\epsilon - 2eV) - n(\epsilon) \big\} \\ & \times A(\boldsymbol{\rho}_1, \boldsymbol{\rho}_2; \epsilon)\, A(\boldsymbol{\rho}_1, \boldsymbol{\rho}_2; 2eV - \epsilon). \end{aligned} \tag{3.14}$$

where $n(\epsilon) \equiv (\exp(\beta\epsilon) + 1)^{-1}$ is the Fermi distribution and $\tilde{\nu}_{\mathrm{P}}$ $[\equiv m/(2\pi\hbar^2 k_{\mathrm{F}})^{-1}$ with k_{F} being the Fermi wave-vector$]$ is the one-dimensional density of states on the P-side.

3.3 Case of clean normal-metal contact

3.3.1 General remarks

In this section we pursue the evaluation of Eq. (3.14) for the case of a normal contact that is perfectly clean, in the sense that the spectral function A^{C} (with the superscript C standing for clean) has the form appropriate for a pure metal:

$$A^{\mathrm{C}}(\mathbf{p};\epsilon) = 2\pi\,\delta^{(3)}(\epsilon_p - \epsilon), \tag{3.15}$$

in which $\epsilon_p \equiv p^2/2m - \mu$. The (three-dimensional) Fourier transform of this quantity is given by

$$\begin{aligned} A^{\mathrm{C}}(\mathbf{r},\mathbf{r}';\epsilon) &\equiv \int \frac{d^3p}{(2\pi\hbar)^3}\, A^{\mathrm{C}}(\mathbf{p};\epsilon)\,\mathrm{e}^{i\mathbf{p}\cdot(\mathbf{r}-\mathbf{r}')/\hbar}, && (3.16)\\ &= \frac{m}{\hbar^2\pi}\frac{\sin\left\{\sqrt{2m\hbar^{-2}(\epsilon+\mu)}|\mathbf{r}-\mathbf{r}'|\right\}}{|\mathbf{r}-\mathbf{r}'|}, && (3.17)\end{aligned}$$

Next, by inserting this expression into Eq. (3.14) and limiting our attention to low temperatures (i.e. $k_{\mathrm{B}}T \ll eV$, with k_{B} being Boltzmann's constant) and low voltages (i.e. $eV \ll \Delta$) [75], we obtain an equation for the low-voltage conductance as a functional of the pseudogap phase-phase correlation function

$$\begin{aligned} \left.\frac{I(V)}{V}\right|_{V\to 0^+} &= \frac{e^2}{\hbar}\left|\frac{t_0 k_{\mathrm{F}} a}{4\pi k_{\mathrm{F}}^2}\right|^4 k_{\mathrm{F}}^2\pi \\ &\times \int_{\mathcal{A}} d^2\rho_1 \int_{\mathcal{A}} d^2\rho_2\; g(\boldsymbol{\rho}_1-\boldsymbol{\rho}_2)\frac{\sin^2 k_{\mathrm{F}}|\boldsymbol{\rho}_1-\boldsymbol{\rho}_2|}{|\boldsymbol{\rho}_1-\boldsymbol{\rho}_2|^2}. \end{aligned} \tag{3.18}$$

3.3.2 Illustrative example: BKT correlations

The main conclusion of Sec. 3.3.1 is that the contribution of Andreev reflection to the tunneling current is sensitive to spatial inhomogeneity of the superconducting phase, such as is proposed to exist in the pseudogap state. For the purposes of illustration, we now examine a specific example of how the current enhancement due to Andreev reflection is increasingly suppressed, with increasing area, due to destructive interference. In this example, we assume that the phase-phase correlations in the pseudogap state are adequately modeled by those associated with the Berezinskiı-Kosterlitz-Thouless (BKT) theory of the two-dimensional XY model [49, 51, 76]. The relevance of this theory to the cuprate materials [77] originates in the fact that their pronounced planar character causes the intermediate length-scale electronic structure to be characterized by two-dimensional XY behavior, which is expected to cross over to three-dimensional XY behavior only very close to the superconducting transition. In order to compute the current for this BKT scenario, we need a form for $g(\boldsymbol{\rho})$. On length-scales short compared with the phase-phase correlation length ξ_ϕ, the function $g(\boldsymbol{\rho})$ approaches unity; on length-scales long compared with ξ_ϕ, it exhibits exponential behavior [76]. As we are only seeking an illustrative computation of the current, the exact details of this crossover are unimportant, and thus we adopt the form

$$g(\boldsymbol{\rho}) = \mathrm{e}^{-|\boldsymbol{\rho}|/\xi_\phi}, \tag{3.19}$$

and we take the interface to have the shape of a disk of radius L. Inserting Eq. (3.19) into Eq. (3.18), we see that the low-voltage Andreev conductance per unit area through the interface has the form

$$\left.\frac{I(V)}{\pi L^2\, V}\right|_{V\to 0^+} = \Gamma_{\mathrm{C}}\, f_{\mathrm{C}}(k_{\mathrm{F}}\xi_\phi, L/\xi_\phi), \tag{3.20}$$

$$\Gamma_{\mathrm{C}} \equiv \frac{e^2}{\hbar}\frac{k_{\mathrm{F}}^2\pi^2}{2}\left|\frac{t_0 k_{\mathrm{F}} a}{4\pi\epsilon_{\mathrm{F}}}\right|^4 \times \ln\left(1+4k_{\mathrm{F}}^2\xi_\phi^2\right), \tag{3.21}$$

$$f_{\mathrm{C}}(k_{\mathrm{F}}\xi_\phi, L/\xi_\phi) \equiv \frac{2}{\pi^2 \ln\left(1+4k_{\mathrm{F}}^2\xi_\phi^2\right)} \times \int_1 d^2x_1 \int_1 d^2x_2\, \frac{\sin^2 k_{\mathrm{F}} L|\mathbf{x}_1-\mathbf{x}_2|}{|\mathbf{x}_1-\mathbf{x}_2|^2}\mathrm{e}^{-|\mathbf{x}_1-\mathbf{x}_2|(L/\xi_\phi)}. \tag{3.22}$$

Here, the subscript 1 indicates that the integrals are taken over disks of unit radius. The prefactor Γ_{C} is the limiting value of the conductance per unit area in the limit of large interface area. [Note that Γ_{C} vanishes for the case of no phase coherence (i.e. $k_{\mathrm{F}}\xi_\phi = 0$).]

One of our primary concerns is how the varying of the interface size would provide information regarding the structure of the phase correlations; this information is contained in the function f_{C}, which depends only on the dimensionless quantities $k_{\mathrm{F}}\xi_{\phi}$ and L/ξ_{ϕ}. For generic values of its arguments, the form of f_{C} can be determined only via numerical integration; however, its behavior can be determined in various physically relevant asymptotic limits. To begin with, let us assume that the phase correlations persist over length-scales that are long compared with the Fermi wavelength on the normal side (i.e. $k_{\mathrm{F}}\xi_{\phi} \gg 1$), and let us consider varying the interface size. For small interface sizes (i.e. $k_{\mathrm{F}}^{-1} \ll L \ll \xi_{\phi}$), f_{C} increases logarithmically with L (i.e. $f_{\mathrm{C}} \approx \ln k_{\mathrm{F}}L/\ln k_{\mathrm{F}}\xi_{\phi}$). In the opposite regime of large interface sizes, we expect that Andreev reflection will occur from independent "domains" of uniform phase (so that, e.g., the doubling of the area should double the conductance). Indeed, for $L \gg \xi_{\phi}$,

$$f_{\mathrm{C}} \approx 1 - \frac{16\,k_{\mathrm{F}}^{2}\,\xi_{\phi}^{2}}{(1+4\,k_{\mathrm{F}}^{2}\,\xi_{\phi}^{2})\ln(1+4\,k_{\mathrm{F}}^{2}\,\xi_{\phi}^{2})}\left(\frac{\xi_{\phi}}{\pi L}\right) \tag{3.23}$$

for any value of $k_{\mathrm{F}}\xi_{\phi}$. Note the logarithmic dependence of f_{C} (and hence the current per unit area) on the contact size L, which is appropriate given the non-classical nature of this mesoscopic contribution to the conductance [68].

To study the behavior of f_{C} for intermediate values of L, we perform the integrals in Eq. (3.22) numerically. In Fig. 3.3, we show $1 - f_{\mathrm{C}}$ as a function of L/ξ_{ϕ} for the case of long-range phase correlations (i.e. $k_{\mathrm{F}}\xi_{\phi} = 100$). Thus, as discussed Sec. 3.1, a series of mesoscopic conductance measurements involving a range of contact sizes is expected to be rather sensitive to the characteristic length-scale of phase correlations in the pseudogap state.

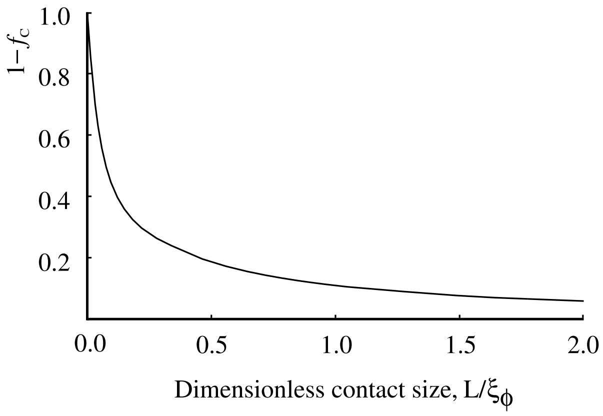

Figure 3.3: $1 - f_{\mathrm{C}}$ (i.e. the departure of the dimensionless Andreev conductance per unit area from its large-area limit) as a function of the dimensionless size of the interface L/ξ_ϕ, for the case of $k_{\mathrm{F}}\xi_\phi = 100$ (computed numerically). For L much smaller than ξ_ϕ, the zero-voltage conductance per unit area is much smaller than its asymptotic value.

3.4 Case of disordered normal-metal contact

3.4.1 General remarks

In Sec. 3.3 we investigated the conductance of a mesoscopic normal metal–to–pseudogap junction for the case of a perfectly clean normal metal. We now address the issue of the sensitivity of the main result (i.e. that this conductance contains information regarding the spatial extent of the pseudogap-side phase correlations) to the assumption that the contact is a perfectly clean metal [78]. Specifically, we examine how Eq. (3.18) is modified by the presence of disorder in the normal-metal contact. As we shall see, in the presence of disorder the most significant contribution to the conductance is associated with so-called Cooperon diagrams, familiar from the theory of the weak-localization corrections to the conductivity of a disordered metal [79].

As is conventional, we take the disorder to be due to uncorrelated point-like impurities, which scatter the electrons elastically. Moreover, we assume that the dephasing length L_ϕ is long, compared to both ξ_ϕ and the mean free path ℓ (which characterizes the strength of the disorder and is related to the scattering time τ via $\ell \equiv v_{\mathrm{F}}\tau$). Although we are focusing on situations in which L_ϕ is larger than the interface size [80], so that one expects substantial sample-to-sample fluctuations (which may in fact be interesting to study), we shall restrict our attention solely to the disorder average of the current. Then, averaging the current in Eq. (3.14) over configurations of the potential scatterers on the normal side, an averaging that we indicate via $\langle \cdots \rangle_{\rm dis}$, we arrive at

$$\begin{aligned}\langle I(V)\rangle_{\rm dis} = \frac{e}{\hbar}\frac{\pi}{8}|t_0 a|^4 \tilde{\nu}_{\rm P}^2 \int_{\mathcal{A}} d^2\rho_1 \int_{\mathcal{A}} d^2\rho_2\, g(\boldsymbol{\rho}_1 - \boldsymbol{\rho}_2) \\ \times \int_{-\mu}^{2eV+\mu} d\epsilon\, \frac{\Delta^2}{\Delta^2 - (eV-\epsilon)^2} \big\{ n(\epsilon - 2eV) - n(\epsilon) \big\} \\ \times \langle A^{\rm D}(\boldsymbol{\rho}_1, \boldsymbol{\rho}_2; \epsilon)\, A^{\rm D}(\boldsymbol{\rho}_1, \boldsymbol{\rho}_2; 2eV - \epsilon) \rangle_{\rm dis}\ ,\end{aligned} \tag{3.24}$$

where the superscript D refers to the disordered case. The disorder-averaged product of spectral functions $\langle A^{\rm D}(\boldsymbol{\rho}_1, \boldsymbol{\rho}_2; \epsilon)\, A^{\rm D}(\boldsymbol{\rho}_1, \boldsymbol{\rho}_2; 2eV - \epsilon) \rangle_{\rm dis}$ contains contributions that extend over length-scales $|\boldsymbol{\rho}_1 - \boldsymbol{\rho}_2|$ much larger than ℓ. These Cooperon contributions provide the mechanism for the transmission of the phase-sensitive information that would be probed in Andreev interferometry experiments involving a disordered normal-metal contact.

3.4.2 Semiclassical picture

Before deriving our result for the contribution of the Cooperon to $\langle I(V)\rangle_{\rm dis}$, we pause to motivate physically why this particular contribution is significant. In the context of weak localization, the Cooperon contribution to the conductance is usefully pictured in terms of constructive interference of pairs of paths involving the scattering of electrons from impurities in reverse order [81]. This interference tends to "localize" electrons, thus causing a reduction in conductivity. In the present context, however, the origin of the Cooperon is slightly different. To see this, consider the amplitude $A^{\bar{\beta}\alpha}_{\mathbf{rx}}$ for an electron at position $\mathbf{x}$ in the normal metal to scatter from a sequence of impurities labeled by the index α, to Andreev reflect at the position $\mathbf{r}$ on the interface, to then scatter from the sequence of impurities labeled $\bar{\beta}$, and finally to return to the position $\mathbf{x}$. Then, the probability for an electron leaving $\mathbf{x}$ and reflecting from the interface to return to $\mathbf{x}$ as a hole is given by the squared modulus of the sum of such amplitudes, i.e.,

$$P(\mathbf{x}) = \Big|\sum_{\alpha\bar{\beta}\mathbf{r}} A^{\bar{\beta}\alpha}_{\mathbf{rx}}\Big|^2 = \sum_{\alpha\bar{\beta}\mathbf{r}} \sum_{\alpha'\bar{\beta}'\mathbf{r}'} \left(A^{\bar{\beta}\alpha}_{\mathbf{rx}}\right)^* A^{\bar{\beta}'\alpha'}_{\mathbf{r}'\mathbf{x}}. \tag{3.25}$$

As is well known, the amplitude $A^{\bar{\beta}\alpha}_{\mathbf{rx}}$ depends sensitively on the specific realization

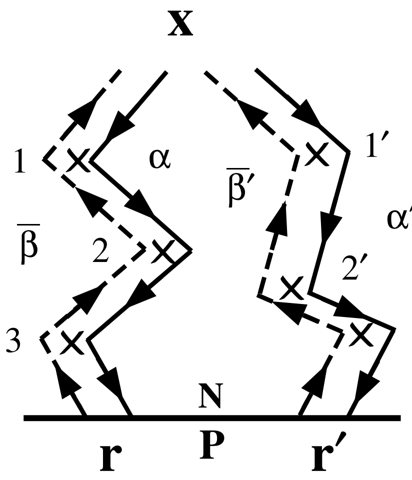

Figure 3.4: Schematic depiction of two semiclassical trajectories in which an electron leaves position $\mathbf{x}$ in the normal region (N), undergoes multiple elastic scattering events, then undergoes Andreev reflection at the NS interface (horizontal line), and then returns to $\mathbf{x}$ as a hole via the same scatterers but in reverse order. Full (dashed) lines represent electron (hole) trajectories; crosses represent impurity scattering potentials.

of the disorder; thus, the right-hand side of Eq. (3.25) contains many terms that are disorder-dependent complex numbers. These contributions to $P(\mathbf{x})$ average to zero upon disorder averaging. However, amongst the collection of amplitudes there is a special subset describing processes in which the hole, as it returns from the interface to $\mathbf{x}$, does so via the same collection of impurities visited by the electron on the outbound segment of the trajectory but in the reverse order. If we denote the reverse of the sequence of impurities $\bar{\beta}$ by the sequence β then this special subset consists of the amplitudes $A^{\alpha\alpha}_{\mathbf{rx}}$; these amplitudes have the form of *real* numbers, regardless of the specific locations of the impurities, except for a factor due to the phase shift associated with Andreev reflection. To see this, consider, e.g., the left-hand pair of paths (electron and hole) in Fig. 3.4. The electron path (full line) originates at $\mathbf{x}$, scatters from impurities at positions 1, 2 and 3, and then Andreev reflects as a hole. The hole then propagates back to $\mathbf{x}$, scattering from the impurities at positions 3, 2 and 1 before returning to the position $\mathbf{x}$. The dynamical phase acquired by the electron as it propagates to the interface is canceled by a phase of the opposite sign acquired by the hole. Thus, the amplitude for an electron at $\mathbf{x}$ to return as a hole at $\mathbf{x}$ depends only on the phase of the condensate at $\mathbf{r}$:

$$A^{\alpha\alpha}_{\mathbf{rx}} \sim \mathrm{e}^{i\phi(\mathbf{r})}. \tag{3.26}$$

Thus, one sees that the most significant contribution to Eq. (3.25) is given approximately by

$$P(\mathbf{x}) \sim \sum_{\mathbf{r},\mathbf{r}'} \mathrm{e}^{i(\phi(\mathbf{r})-\phi(\mathbf{r}'))}, \tag{3.27}$$

and hence that $P(\mathbf{x})$ is sensitive to the nature of the pseudogap phase-phase correlations, a sensitivity similar to that embodied in Eq. (3.18).

3.4.3 Microscopic calculation

The explicit computation of the contribution of the Cooperon directly follows the usual analysis found in the context of weak localization; following Rammer [79], we find that the disorder-averaged product of spectral functions has the form

$$\begin{aligned} &\left\langle A^{\mathrm{D}}(\mathbf{x},\mathbf{x}',\epsilon)A^{\mathrm{D}}(\mathbf{x},\mathbf{x}',\epsilon')\right\rangle_{\mathrm{dis}} \\ &= \frac{2\pi}{\hbar}\nu_{\mathrm{N}}\int \frac{d^3Q}{(2\pi\hbar)^3}\mathrm{e}^{i\mathbf{Q}\cdot(\mathbf{x}-\mathbf{x}')/\hbar}\left\{C(\mathbf{Q},\epsilon-\epsilon')+C(\mathbf{Q},\epsilon'-\epsilon)\right\}, \end{aligned} \tag{3.28}$$

where the Cooperon propagator $C(\mathbf{Q},w) \equiv (-i\omega/\hbar + DQ^2\hbar^{-2})^{-1}$, the diffusion constant $D \equiv v_{\mathrm{F}}^2\tau/3$ (in three dimensions), and $\nu_{\mathrm{N}}[\equiv k_{\mathrm{F}}m/(2\pi^2\hbar^2)]$ is the normal-side density of states. Inserting Eq. (3.28) into Eq. (3.24) leads to the expression

$$
\begin{aligned}
\langle I(V)\rangle_{\text{dis}} = e\left|\frac{t_0 k_{\text{F}} a}{4\pi k_{\text{F}}^2}\right|^4 \frac{\pi^2 k_{\text{F}}^3}{2m}\int_{\mathcal{A}} d^2\rho_1 \int_{\mathcal{A}} d^2\rho_2\; g(\boldsymbol{\rho}_1-\boldsymbol{\rho}_2) \\
\times \int_{-\mu_{\text{N}}}^{2eV+\mu_{\text{N}}} d\epsilon\,\big\{n(\epsilon-2eV)-n(\epsilon)\big\}\frac{\Delta^2}{\Delta^2-(eV-\epsilon)^2} \\
\times\big\{C\big(\boldsymbol{\rho}_1-\boldsymbol{\rho}_2, 2(eV-\epsilon)\big)+C\big(\boldsymbol{\rho}_1-\boldsymbol{\rho}_2, 2(\epsilon-eV)\big)\big\},
\end{aligned}
\tag{3.29}
$$

where $C\big(\boldsymbol{\rho},\epsilon\big)$ is the (three-dimensional) Fourier transform of $C\big(\mathbf{Q},\epsilon\big)$.

To analyze $\langle I(V)\rangle_{\text{dis}}$ we make two further simplifying assumptions. First, as in the clean case, we limit our attention to low temperatures (i.e. $k_{\text{B}}T \ll eV$), and thus we obtain

$$
\begin{aligned}
\langle I(V)\rangle_{\text{dis}} \approx \frac{e}{\hbar}\left|\frac{t_0 k_{\text{F}} a}{4\pi k_{\text{F}}^2}\right|^4 \frac{\pi\hbar}{4mD}k_{\text{F}}^3\int_0^{2eV} d\epsilon\,\frac{\Delta^2}{\Delta^2-(eV-\epsilon)^2} \\
\times\int_{\mathcal{A}} d^2\rho_1\int_{\mathcal{A}} d^2\rho_2\,\frac{g(\boldsymbol{\rho}_1-\boldsymbol{\rho}_2)}{|\boldsymbol{\rho}_1-\boldsymbol{\rho}_2|}\mathrm{e}^{-\sqrt{(\hbar D)^{-1}|eV-\epsilon|}|\boldsymbol{\rho}_1-\boldsymbol{\rho}_2|} \\
\times\cos\big\{\sqrt{(\hbar D)^{-1}|eV-\epsilon|}|\boldsymbol{\rho}_1-\boldsymbol{\rho}_2|\big\},
\end{aligned}
\tag{3.30}
$$

where we have inserted the explicit real-space expression for the Cooperon. Second, by making the restriction to low voltages (i.e. $eV \ll \Delta$) [75], we may in Eq. (3.30) replace $\Delta^2/(\Delta^2-(eV-\epsilon)^2)$ by 1. Furthermore, in the presence of disorder one has the natural length-scale $L_V \equiv \sqrt{\hbar D/eV}$. At sufficiently low voltages and small interface sizes, L_V will be much larger than typical values of $|\boldsymbol{\rho}_1-\boldsymbol{\rho}_2|$, so that one may expand to lowest order in L/L_V, thus obtaining

$$
\begin{aligned}
&\langle I(V)\rangle_{\text{dis}} \\
&\quad\approx\frac{e^2}{\hbar}V\left|\frac{t_0 k_{\text{F}} a}{4\pi k_{\text{F}}^2}\right|^4\frac{\pi k_{\text{F}}}{L_{\text{F}}^2 L_V}\int_{\mathcal{A}} d^2\rho_1\int_{\mathcal{A}} d^2\rho_2\; g(\boldsymbol{\rho}_1-\boldsymbol{\rho}_2) \\
&\quad\left\{\frac{L_V}{|\boldsymbol{\rho}_1-\boldsymbol{\rho}_2|}+\mathcal{O}(1)\right\},
\end{aligned}
\tag{3.31}
$$

where $L_{\text{F}} \equiv \sqrt{\hbar D/k_{\text{F}}^2}$. Thus, as found in Sec. 3.3 for the case of a clean normal metal contact, the low-voltage conductance of a disordered metal–to–pseudogap junction also contains information regarding the pseudogap phase-phase correlation function.

3.4.4 Illustrative example: BKT correlations

In this section we examine the area-dependence of the low-temperature and low-voltage conductance of a disordered normal metal–to–pseudogap junction for the case of BKT correlations. As in Sec. 3.3, we assume that phase correlations decay in an exponential fashion, consistent with the BKT scenario. Our starting point is thus Eq. (3.31), together with the model of phase correlations given by Eq. (3.19). By considering the $V \to 0^+$ behavior of Eq. (3.31) we arrive at the low-temperature conductance per unit area (for the case of an interface having the shape of a disk of radius L):

$$\left.\frac{\langle I(V)\rangle_{\rm dis}}{\pi L^2 V}\right|_{V\to 0^+} \approx \Gamma_{\rm D}\, f_{\rm D}(L/\xi_\phi), \tag{3.32}$$

$$\Gamma_{\rm D} \equiv \frac{e^2}{\hbar}\left|\frac{t_0 k_{\rm F} a}{4\pi k_{\rm F}^2}\right|^4 \frac{2\pi^2 k_{\rm F}\xi_\phi}{L_{\rm F}^2}, \tag{3.33}$$

$$f_{\rm D} \equiv \frac{1}{2\pi^2}\left(\frac{L}{\xi_\phi}\right)\int_1 d^2x_1 \int_1 d^2x_2 \frac{{\rm e}^{-|\mathbf{x}_1-\mathbf{x}_2|(L/\xi_\phi)}}{|\mathbf{x}_1-\mathbf{x}_2|}. \tag{3.34}$$

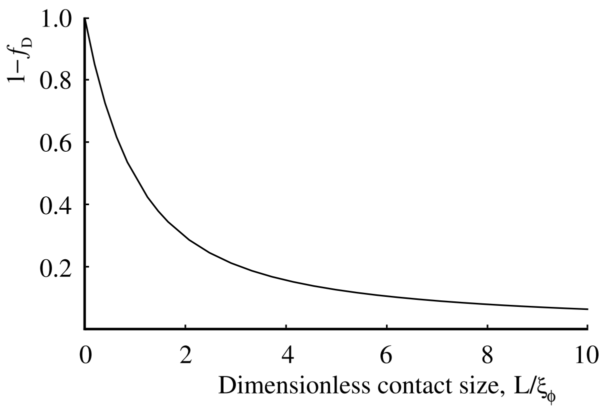

Figure 3.5: $1 - f_{\rm D}$ (i.e. the departure of the dimensionless Andreev conductance per unit area from its large-area limit) as a function of the dimensionless size of the interface L/ξ_ϕ for the case of a disordered normal-metal contact. For L much smaller than ξ_ϕ, the zero-voltage conductance per unit area is much smaller than its asymptotic value.

By evaluating the integrals in Eq. (3.34), we obtain

$$f_{\rm D} = 1 + \left(\frac{\xi_\phi}{L}\right)\left\{L_1\left(\frac{2L}{\xi_\phi}\right) - I_1\left(\frac{2L}{\xi_\phi}\right)\right\} \tag{3.35}$$

where I_1 is a modified Bessel function and L_1 is a modified Struve function. The asymptotic behavior of f_{D} is linear for small L (i.e. $f_{\mathrm{D}} \approx (8/3\pi)(L/\xi_\phi)$ for $L/\xi_\phi \ll 1$); for large L it approaches unity as an inverse power of L [i.e. $f_{\mathrm{D}} \approx 1 - (2\xi_\phi/\pi L)$ for $L/\xi_\phi \gg 1$]. In Fig. 3.5 we show how this function crosses over between these two limits. As with the case of the clean contact, the conductance shows marked sensitivity to the phase-phase correlations of the pseudogap state.

3.5 Concluding remarks

In this chapter we have proposed and explored theoretically the possibility of using Andreev interferometry to probe the spatial structure of the phase correlations in the pseudogap state of the cuprate superconductors. The viability of this technique rests on the sensitivity of the tunneling current across mesoscopic normal–to–pseudogap junctions to spatial variations in the local superconducting order in the pseudogap state, as well as the possibility of using junctions having a range of areas. The picture of the pseudogap state to which our approach directly applies is one in which phase correlations extend over length-scales that are considerably larger than the characteristic dimension of a charge-carrier pair. If this is not the case then the intervortex spacing becomes comparable to the vortex core size, a substantial fraction of the electrons tunneling from the contact encounter vortex cores, and our formalism would have to be extended to account for the associated variation of the amplitude of the superconducting order parameter.

By considering a simple tunneling model, we have established a relationship between the tunneling current and the equilibrium phase-phase correlator characterizing the pseudogap state. We have considered the cases in which the normal region (i.e. the contact) is either a clean or a disordered metal. In both cases, we have assumed that phase coherence length for quasiparticles on the *normal* side is greater than the contact size. If this condition is not met, then, throughout our results, the contact size must be replaced by the dephasing length.

Up to this point we have not paid any attention to the fact that the pairing state is, in all likelihood, d-wave. Assuming that this is indeed the case, there are certain additional factors that may complicate the task of conclusively extracting information via Andreev interferometry. Specifically, these complications are: (i) the presence of low-lying quasiparticle states near the nodes of the gap; and (ii) Andreev bound states [33], localized at the surface, arising from the sign change in the pair potential. Both complications lead to nonzero quasiparticle contributions to the current, and may obscure the contribution due to Andreev reflection. We propose two methods to circumvent these difficulties: (i) tunneling into the antinodal direction, so as to minimize the magnitude of the contributions associated with the above-mentioned complications; and (ii) separating the quasiparticle contribution from the Andreev contribution via their characteristic temperature dependences. Method (i) relies on the notion that by choosing an experimental geometry such that the antinodal direction is normal to the plane of the interface, electrons incident from the normal side will tunnel into a particular "cone" of momentum states in the pseudogap material. Hence, the coupling to nodal states can be minimized. Furthermore, with this geometry, quasiparticle states that reflect specularly from the surface do not encounter a sign change in the d-wave order parameter, and thus there are no Andreev bound states. Indeed, the experiments of Wei et al. [82] have found that by using a contact oriented normal to the antinodal direction the contribution due to the Andreev bound states is minimized. Method (ii) makes use of the fact that, near T_{c}, the quasiparticle contribution to the current varies only weakly with temperature. In contrast, the Andreev contribution to the current is expected to increase sharply with decreasing temperature (i.e. as $T \to T_{\mathrm{c}}$ from above) because the associated increase in ξ_{ϕ} lessens the effects of destructive interference.

Let us note, in passing, that we expect the results in the present chapter to be at least *qualitatively* valid for regimes in which the tunneling barrier is small and, hence, the Andreev current through the interface is large. In such regimes, the contribution to the current due to Andreev reflection will, in fact, be much larger than the contribution from quasiparticle tunneling. However, to arrive at a quantitative theory for this case one would have to extend the approach taken here by going beyond simple perturbation theory in the normal-to-pseudogap tunneling amplitude.

To illustrate this Andreev interferometry proposal, we have applied our general results to a simple model of the pseudogap phase-phase correlations, which is intended to mimic the BKT correlations relevant to certain proposed pictures of the pseudogap state. Our considerations suggest that measurements of the low-voltage conductance of mesoscopic junctions of varying areas between normal-state and pseudogap-state regions would reveal information about the phase-phase correlations in the pseudogap state.

Chapter 4

Intrinsic resistivity and the SO(5) theory of high-temperature superconductivity

4.1 Introduction

As discussed in Sec. 1.4, Zhang's approach to the physics of the high-temperature superconductors [9] is rooted in the observation that the phase diagram of these materials contains nearby regions of antiferromagnetism and superconductivity. This has led Zhang to propose a low-energy effective description of these materials that combines the U(1) symmetry sector associated with the superconductivity with the SO(3) symmetry sector associated with the antiferromagnetism, SO(5) being the minimal symmetry group that admits this combination. In the resulting description, the state of the system is characterized, locally, by a five-dimensional "superspin," subject to a symmetry-reducing term that favors one or other of the sectors, U(1) or SO(3). The superspin is constrained to have unit magnitude, which is appropriate for temperatures sufficiently low that fluctuations in the magnitude of the superspin are negligible. The possibility of rotations between the U(1) and SO(3) sectors is where a number of the unusual consequences of Zhang's approach lie [83–85].

It has long been appreciated [86, 87] that in conventional superconductors topologically accessible fluctuations in the *amplitude* of the superconducting order parameter provide an intrinsic mechanism via which supercurrent can be dissipated in a thin wire. A uniform current-carrying state characterized by a specific uniform phase-gradient along the wire is only *metastable*, thermodynamically, so that by undergoing amplitude-reducing thermal fluctuations the system can decrease its current. In the present Chapter we investigate a related intrinsic dissipation mechanism appropriate for the superconducting state of the SO(5) model of high-temperature superconducting materials. In this case, the relevant dissipative process is a fluctuation in the *orientation* of the superspin, during which the system temporarily becomes antiferromagnetic along a small segment of the wire, allowing the analogue of a phase-slip process to occur. Such fluctuations are equivalent to the passing of superconducting vortices with antiferromagnetic cores [83] across the wire. Related dissipative processes have been addressed in the context of superfluid ^{3}He-A [88] and (for appropriate values of the gradient coupling constants) thin tubes of nematic liquid crystal [89]. By constructing a version of the approach to intrinsic dissipation pioneered by Langer and Ambegaokar for conventional superconductors [87], suitably modified for the SO(5) model of superconductivity, we shall estimate the free-energy barrier for this type of fluctuation and, hence, arrive at an estimate of the current-voltage relationship for a sufficiently thin wire.

The research presented in this Chapter has been reported in Ref. [90].

4.2 SO(5) theory

In Zhang's theory of high-temperature superconductivity and antiferromagnetism, the local state of the system at the spatial position $\mathbf{r}$ is determined by a five-component unit-vector field $\mathbf{n}(\mathbf{r})$ such that the components n^1, n^2 and n^3 together specify the antiferromagnetic Néel vector, and the components n^4 and n^5 together specify the amplitude and phase of the superconducting order. The constraint on the magnitude of $\mathbf{n}$ implements the notion that the enhancement of antiferromagnetic order is necessarily accompanied by the diminution of superconducting order, and vice versa. As discussed in Sec. 1.4, the SO(5) free-energy density f comprises an isotropic gradient term along with a symmetry-reducing term:

$$f = \frac{\rho}{2}\sum_{a=1}^{5} \partial_\mu n^a \, \partial_\mu n^a - \frac{g}{2}\sum_{a=1}^{3} (n^a)^2 \,. \tag{4.1}$$

Here, the (real-space) subscript μ runs from 1 to 3 (or x, y, z), repeated indices being summed over. The (chemical-potential dependent) parameter g [91] governs whether the stable homogeneous state is superconducting ($g < 0$), as we select in the present chapter, or antiferromagnetic ($g > 0$). We parameterize $\mathbf{n}$ via the angles $\{\tilde{\theta}, \tilde{\phi}, \tilde{\psi}, \tilde{\chi}\}$ such that

$$\begin{aligned} n^1 &= \sin\tilde{\theta}\cos\tilde{\psi}\cos\tilde{\chi}, & n^4 &= \cos\tilde{\theta}\cos\tilde{\phi}, \\ n^2 &= \sin\tilde{\theta}\cos\tilde{\psi}\sin\tilde{\chi}, & n^5 &= \cos\tilde{\theta}\sin\tilde{\phi}. \\ n^3 &= \sin\tilde{\theta}\sin\tilde{\psi}, & & \end{aligned}$$

The angle $\tilde{\theta}$ measures the relative amount of antiferromagnetic versus superconducting order (without regard for the orientation of the antiferromagnetism or the phase of the superconductivity), with $\tilde{\theta} \equiv 0$ in the purely superconducting state. In addition, $\tilde{\phi}$ is the phase of the superconductivity, and $\tilde{\psi}$ and $\tilde{\chi}$ specify the orientation of the antiferromagnetic Néel vector.

4.3 Thin superconducting wire

Let us suppose that the system consists of a wire of length L, sufficiently long and narrow that we may assume that $\{\tilde{\theta}, \tilde{\phi}, \tilde{\psi}, \tilde{\chi}\}$ do not vary in the directions transverse to the wire (i.e. in the y or z directions). Under these circumstances f becomes

$$\begin{aligned} f &= (\rho/2)\big\{(\partial_x\tilde{\theta})^2 + (\partial_x\tilde{\phi})^2\,\cos^2\tilde{\theta} + (\partial_x\tilde{\psi})^2\,\sin^2\tilde{\theta} \\ &\qquad +(\partial_x\tilde{\chi})^2\,\sin^2\tilde{\theta}\cos^2\tilde{\psi}\big\} + (|g|/2)\sin^2\tilde{\theta} \qquad (4.2) \\ &= (|g|/2)\,\big\{(\partial_\tau\theta)^2 + (\partial_\tau\phi)^2\,\cos^2\theta + (\partial_\tau\psi)^2\,\sin^2\theta \\ &\qquad +(\partial_\tau\chi)^2\,\sin^2\theta\cos^2\psi + \sin^2\theta\big\}\,. \qquad (4.3) \end{aligned}$$

To obtain Eq. (4.3) we have exchanged the independent variable x for its dimensionless counterpart τ, defined via $\tau \equiv x/\xi_\pi$, where $\xi_\pi \equiv \sqrt{\rho/|g|}$ is the correlation length for antiferromagnetic fluctuations, which sets the length-scale for dissipative events. Furthermore, we have defined the function θ such that $\theta(\tau) \equiv \tilde{\theta}(x)$, and similarly for ϕ, ψ and χ. The quantity ℓ will denote the dimensionless length of the wire, i.e. $\ell \equiv L/\xi_\pi$.

In order to estimate the rate at which current-dissipating processes occur we compute the height of the free-energy barrier opposing them. To do this we follow Langer and Ambegaokar [87] and seek the metastable (i.e. uniform, current-carrying) states between which the system fluctuates, and the transition (i.e. unstable saddle-point) states through which the system passes as current is dissipated. Both classes of states, metastable and transition, are stationary configurations of the free energy, and therefore obey the corresponding Euler-Lagrange equations. These equations may be simplified, however, due to the homogeneity (i.e. τ-independence) and gauge-invariance in the superconducting sector (i.e. ϕ-independence) of f. The former symmetry leads to the existence of the first integral

$$\dot{\theta}^2+\dot{\phi}^2\cos^2\theta+\dot{\psi}^2\sin^2\theta+\dot{\chi}^2\sin^2\theta\cos^2\psi-\sin^2\theta \equiv \epsilon, \qquad (4.4)$$

where overdots denote derivatives with respect to τ, and ϵ is constant. The latter symmetry leads to the existence of a cyclic coordinate, so that

$$\dot{\phi}\cos^2\theta \equiv I\,. \qquad (4.5)$$

Here, the dimensionless supercurrent density I, in terms of which the dimensionful supercurrent density J is given by $J = 2e\rho I/\hbar\xi_\pi$, is constant. By replacing $\dot{\phi}$ in Eq. (4.4) with I, using Eq. (4.5), we obtain

$$\dot{\theta}^2 + \frac{I^2}{\cos^2\theta} + \dot{\psi}^2 \sin^2\theta + \dot{\chi}^2 \sin^2\theta \cos^2\psi - \sin^2\theta = \epsilon \,. \tag{4.6}$$

The relevant supercurrent-carrying metastable states are solutions of Eq. (4.4) and Eq. (4.5) for which $\theta(\tau) \equiv 0$ (and therefore ψ and χ play no role) and $\dot{\phi} = I$. We refer to these states as "uniformly winding" because in them ϕ increases linearly with position along the sample. As for the transition states, we assume that they possess appreciable antiferromagnetic order only within a small segment of the wire, and that elsewhere θ is negligibly small. Furthermore, the orientation of the antiferromagnetic order generated during the fluctuation is uniform, because transition states with inhomogeneous antiferromagnetic orientation would have higher free energy, and would correspondingly occur less frequently. Therefore we only consider transition states for which $\dot{\psi} \equiv \dot{\chi} \equiv 0$. Thus, by applying Eq. (4.6) far from the antiferromagnetic region we determine that

$$I^2 = \epsilon \,. \tag{4.7}$$

Let us denote the extreme value of $\theta(\tau)$ by θ_0, and let us suppose that it occurs at the location $\tau = \tau_0$. At this location $\dot{\theta} = 0$, so that Eq. (4.6), combined with Eq. (4.7), gives

$$\dot{\theta}^2 = \sin^2\theta - I_{\mathrm{t}}^2 \tan^2\theta \,, \tag{4.8}$$

$$I_{\mathrm{t}}^2 = \cos^2\theta_0 \,. \tag{4.9}$$

By integrating Eq. (4.8) we find

$$\sin\theta(\tau) = \sin\theta_0 \sqrt{1 - \tanh^2[(\tau - \tau_0)\sin\theta_0]} \,. \tag{4.10}$$

Finally, by using Eq. (4.5), along with Eq. (4.10), we obtain

$$\begin{aligned}\phi(\tau) - \phi(\tau_0) &= I_{\rm t} \int_{\tau_0}^{\tau} d\tau' / \cos^2\theta(\tau') \\ &= I_{\rm t}(\tau - \tau_0) + \arctan\left\{\tan\theta_0 \tanh\left[(\tau - \tau_0)\sin\theta_0\right]\right\}.\end{aligned} \tag{4.11}$$

Thus we see that far from τ_0 (i.e. far from the center of the fluctuation) the transition

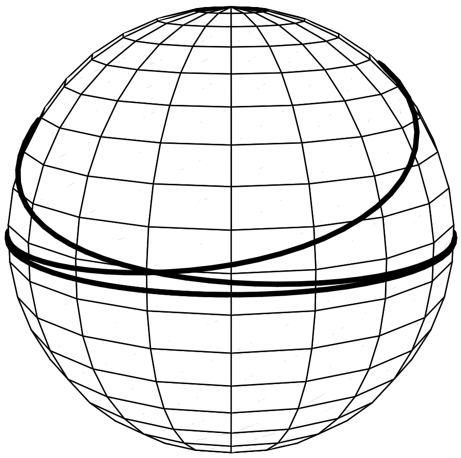

Figure 4.1: Parametric plot of a typical (partially antiferromagnetic) transition state (full curve) on the surface of the unit 2-sphere in the space spanned by $\{n^4, n^5, \sin\theta\}$. Trajectories of the (purely superconducting) metastable states lie on the equator of this sphere, for which $\theta = 0$.

states wind uniformly, as do the metastable states. However, in the transition states the order parameter undergoes an orientational distortion over a length of order ξ_π that takes θ out of the $\theta = 0$ plane. Thus, a given transition state possesses a region of antiferromagnetic order in a fixed but arbitrary direction. Indeed, there is a family of symmetry-related transition states generated by changing this direction, just as there is a family of transition states generated by the (arbitrary) location of τ_0 and the (arbitrary) overall phase. An example of a transition state is shown in Fig. 4.1. Hence we see that the relevant fluctuation for SO(5) superconductors is one in which supercurrent can be dissipated via a thermally activated process in which a "loop" of order parameter passes over the order-parameter sphere, so that the total phase difference (and hence supercurrent in the resulting metastable state) is reduced by

2π. Intuitively, it seems reasonable that if the "anisotropy" g is not too large (it being adjustable by changing the chemical potential) then this type of fluctuation should be less energetically costly than amplitude fluctuations, and should hence provide the dominant pathway for dissipation. Having determined the form of the metastable and transition states, we now identify the particular transition state through which the system passes as current is dissipated from a given metastable state. In passing from a metastable state to the corresponding transition state, en route to diminishing the current, the superspin nowhere becomes entirely antiferromagnetic (i.e. $|\theta| < \pi/2$). [The transition state represents a configuration in which a loop is about to pass over the order parameter sphere, but has not yet done so.] Thus, if we consider a transition from one metastable state (which we refer to as the "upper metastable state") to a metastable state with 2π less total phase difference (the "lower metastable state") then the actual loss of the phase will occur in passing from the transition state to the lower metastable state. Therefore, the total phase-difference across the sample $\Delta\phi$ is the same in the transition state and the upper metastable state, so that

$$\int_0^\ell d\tau\, \dot{\phi}_{\mathrm{m}} = \Delta\phi = \int_0^\ell d\tau\, \dot{\phi}_{\mathrm{t}}\,, \tag{4.12}$$

where $\phi_{\mathrm{m}}(\tau)$ is the phase of the uniform metastable state and $\phi_{\mathrm{t}}(\tau)$ is the phase of the transition state. This formula provides a connection between the current in the upper metastable state I_{m}^{+} and that in the transition state I_{t}. The left-most term in this equation is given by $I_{\mathrm{m}}^{+}\ell$, which follows readily from the uniformly twisting character of the metastable states. The right-most term may be evaluated via Eq. (4.11), which gives $I_{\mathrm{t}}\ell + 2\theta_0$, or equivalently, using Eq. (4.9), $I_{\mathrm{t}}\ell + 2\arccos I_{\mathrm{t}}$. Thus we arrive at an implicit equation for I_{t} in terms of I_{m}^{+}:

$$I_{\mathrm{m}}^{+}\,\ell - I_{\mathrm{t}}\,\ell = 2\arccos I_{\mathrm{t}} \geq 0\,. \tag{4.13}$$

4.4 Calculation of transition rate

In this section we use Arrhenius rate-law considerations to develop the transition rate. To do this, we need expressions for the free energies of the upper (+) and lower (−) metastable states, as well as of the transition state connecting them. From Eq. (4.3) and the form of the upper and lower metastable states we integrate over the volume of the wire to obtain expressions for the free energies $F_{\mathrm{m}}^{\pm}$ of the these states:

$$F_{\mathrm{m}}^{\pm} = (|g|/2) A\, \xi_{\pi}\, \ell \left(I_{\mathrm{m}}^{\pm}\right)^2 . \tag{4.14}$$

Here, I_{m}^{-} $(= I_{\mathrm{m}}^{+} - 2\pi/\ell)$ is the current in the lower metastable state and A is the cross-sectional area of the wire. Similarly, the free-energy density of the transition states f_{t} may be obtained using Eqs. (4.3), (4.5) and (4.8):

$$f_{\mathrm{t}} = (|g|/2)\, (I^2 + 2\sin^2\theta)\, . \tag{4.15}$$

By integrating Eq. (4.15) over the volume of the wire we arrive at an expression for the free energy F_{t} of the transition state:

$$\begin{aligned} F_{\mathrm{t}} &= (|g|/2) A\, \xi_{\pi} \Big\{ \ell\, I_{\mathrm{t}}^2 + 2 \int_0^{\ell} d\tau\, \sin^2\theta(\tau) \Big\} && (4.16) \\ &= (|g|/2) A\, \xi_{\pi} \left\{ \ell\, I_{\mathrm{t}}^2 + 4\sqrt{1 - I_{\mathrm{t}}^2} \right\} . && (4.17) \end{aligned}$$

By using Eqs. (4.14) and (4.17) we obtain an expression for the free energy barrier ΔF for current dissipation,

$$\Delta F \equiv F_{\mathrm{t}} - F_{\mathrm{m}}^{+} = \frac{|g|}{2} A \xi_{\pi} \Big\{ \ell\, I_{\mathrm{t}}^2 - \ell\, (I_{\mathrm{m}}^{+})^2 + 4\sqrt{1 - I_{\mathrm{t}}^2} \Big\} ,$$

which may be simplified by using the relation (4.13) between I_{t} and I_{m}^{+}. By restricting our attention to states in which the phase winds many times along the wire (i.e. $2 \arccos I_{\mathrm{t}} \ll I_{\mathrm{t}}\, \ell$) we obtain $I_{\mathrm{t}}^2 - (I_{\mathrm{m}}^{+})^2 \simeq -4\ell^{-1} I_{\mathrm{t}} \arccos I_{\mathrm{t}}$, and thus ΔF becomes

$$\Delta F = |g|\, A\, \xi_{\pi} \left\{ -\, 2\, I_{\mathrm{t}} \arccos I_{\mathrm{t}} + 2\sqrt{1 - I_{\mathrm{t}}^2} \right\} . \tag{4.18}$$

It should be noted that $I_{\rm t} = 1$ is the critical current, in the sense that uniformly twisted states with larger values of the current are unstable rather than metastable. For later use, we note that for currents slightly smaller than critical ΔF in the SO(5) model is given by

$$\Delta F \simeq 2\sqrt{2}\,|g|\,A\,\xi_\pi\,(1-I_{\rm t})^{3/2}\,, \tag{4.19}$$

whereas the corresponding expression for conventional superconductors [87] is

$$\Delta F \simeq \sqrt{2}\,(8/3)^{5/4} A\,\xi\,(g_{\rm n}-g_{\rm s})\,(1-I)^{5/4}\,. \tag{4.20}$$

Here, $(g_{\rm n} - g_{\rm s})$ represents the free-energy cost of amplitude fluctuations, and is the analogue of the parameter g within the present theory, and ξ is the superconducting fluctuation correlation length.

To compute the rates of current-decreasing and current-increasing fluctuations we follow LA by assuming that these rates depend exponentially on the free-energy barrier heights. Specifically, the rate $\Gamma(I_{\rm m}^{+} \to I_{\rm m}^{-})$ at which current-decreasing fluctuations occur is given by

$$\begin{aligned}\Gamma(I_{\rm m}^{+} \to I_{\rm m}^{-}) &= \Gamma_0 \exp\{-\beta\,\Delta F) \\ &= \Gamma_0 \exp\left\{-\beta\,|g|\,A\,\xi_\pi\left(-2I_{\rm t}\arccos I_{\rm t} + 2\sqrt{1-I_{\rm t}^2}\right)\right\},\end{aligned} \tag{4.21}$$

where $\beta = 1/k_{\rm B}T$ measures the inverse temperature and Γ_0 is an attempt frequency for dissipative fluctuations. Current-increasing fluctuations, in which the system passes from the lower metastable state to the upper metastable state, also occur. However, these fluctuations have a higher barrier opposing them (i.e. for them $\Delta F \to \Delta F + F_{\rm m}^{+} - F_{\rm m}^{-}$), and thus occur at a lower rate. By using Eq. (4.14) we therefore obtain

$$\begin{aligned}&\Gamma(I_{\rm m}^{+} \leftarrow I_{\rm m}^{-}) = \\ &\Gamma_0 \exp\Big\{-\beta|g|A\,\xi_\pi\Big(-2I_{\rm t}\arccos I_{\rm t} + 2\sqrt{1-I_{\rm t}^2} + 2\pi I_{\rm m}^{+}\Big)\Big\}.\end{aligned} \tag{4.22}$$

The application of a voltage difference ΔV between the ends of the sample causes $\Delta\phi$ to increase linearly with time [i.e. $d(\Delta\phi)/dt = 4\pi e\,\Delta V/h$, where h is Planck's constant and $-e$ is the electronic charge] [92]. In steady state, this will be balanced by the net rate Γ_{net} at which current-decreasing fluctuations occur, i.e.,

$$\Gamma_{\mathrm{net}} = \Gamma(I_{\mathrm{m}}^{+} \rightarrow I_{\mathrm{m}}^{-}) - \Gamma(I_{\mathrm{m}}^{+} \leftarrow I_{\mathrm{m}}^{-}) = \frac{1}{2\pi}\frac{d(\Delta\phi)}{dt}\,. \tag{4.23}$$

The difference between I_{t} and I_{m}^{+} is of order ℓ^{-1}, and we shall henceforth neglect it; thus we simply refer to the current I. This leads to the following expression for the voltage between the ends of the wire in terms of the current along it:

$$\begin{aligned} \Delta V = (h/e)\,\Gamma_0\,\sinh\{\pi\beta|g|A\xi_\pi\, I\} \\ \times \exp\left\{-\beta|g|A\,\xi_\pi\left(-2I\arccos I + 2\sqrt{1-I^2} + \pi I\right)\right\}\,. \end{aligned} \tag{4.24}$$

The corresponding expression for conventional superconductors may be found in Eq. (2.12) of Ref. [87]. As the length-scale of the fluctuation is ξ_π it is natural for ΔV to depend exponentially on $\beta|g|A\xi_\pi$ (i.e. the condensation energy in a correlation length per $k_{\mathrm{B}}T$). Following McCumber and Halperin [93], we estimate Γ_0 to be of order N/τ, where $N \equiv 4\pi L/\xi_\pi$ reflects the range of possible locations along the wire at which the fluctuation may occur (L/ξ_π), as well as the variety of possible Néel-vector orientations (4π). For conventional superconductors τ diverges as $T \rightarrow T_{\mathrm{c}}$. For the SO(5) model we expect τ to diverge as the chemical potential approaches its critical value.

It may be useful to compare expression (4.24) for ΔV with that obtained in Refs. [87, 93] for the case of conventional superconductors. Within the SO(5) model the expression for ΔV in terms of the dimensionful supercurrent density J is given, for $J \simeq J_{\mathrm{c}}$, by

$$\begin{aligned} \Delta V \simeq (h/e)\,\Gamma_0\,\sinh\{\beta AhJ/4e\} \\ \times \exp\left\{-\beta A\left((hJ/4e) + 2\sqrt{2}\,|g|\,\xi_\pi\,(1-J/J_{\mathrm{c}})^{\frac{3}{2}}\right)\right\}\,, \end{aligned} \tag{4.25}$$

whereas the corresponding expression obtained in Refs. [87, 93] is given, for $J \simeq J_{\rm c}$, by

$$\begin{aligned} \Delta V \simeq\, & (h/e)\,\Omega_0\, \sinh\{\beta A h J/4e\} \\ & \times \exp\Big\{-\beta A\Big((hJ/4e)+\sqrt{2}(8/3)^{\frac{5}{4}}\xi(g_{\rm n}-g_{\rm s})(1-J/J_{\rm c})^{\frac{5}{4}}\Big)\Big\}\,. \end{aligned} \tag{4.26}$$

(We have ignored the current dependence of the attempt frequency Ω_0 obtained in Ref. [93].) We see that in this regime the primary qualitative distinction between formulas (4.25) and (4.26) comes from the distinction between the nature of the fluctuations, and the resulting difference between the barrier heights.

4.5 Concluding remarks

We conclude by noting that for conventional superconductors LA [87] have obtained, as a condition for the validity of their approach, the constraint that the wire be thinner than the temperature-dependent superconducting correlation length ξ. (To accomplish this they consider the second variation of the free energy, and require that the transition state be unstable in only one direction in configuration space.) We emphasize that the corresponding condition in the context of the SO(5) theory of high-temperature superconductivity is that the wire be thinner than the correlation length for orientation fluctuations of the superspin, i.e., ξ_π. This length ξ_π is expected to diverge when the chemical potential approaches the superconductor-to-antiferromagnet phase boundary.

Chapter 5

Antiferromagnetic hedgehogs with superconducting cores

5.1 Introduction

In Zhang's SO(5)-symmetry–based approach to the physics of high-temperature superconducting materials [9], the local state of the system at the spatial point $\mathbf{r}$ is characterized by the orientation of a five-component unit vector $\mathbf{n}(\mathbf{r})$. Orientations for which $\sum_{a=1}^{3}(n^a)^2 = 0$ are purely superconducting, the orientation of $\mathbf{n}$ in the (two-dimensional) 4-5 hyperplane determining the phase of the complex superconducting order parameter. Orientations for which $\sum_{a=4}^{5}(n^a)^2 = 0$ are purely antiferromagnetic, the orientation of $\mathbf{n}$ in the (three-dimensional) 3-4-5 hyperplane determining the direction in real space of the antiferromagnetic (i.e., Néel) vector order parameter. The novelty of Zhang's approach lies in its assembling of these two order parameters into a unified order parameter $\mathbf{n}$, and the consequent possibility of orientations of $\mathbf{n}$ that do not lie wholely in one or other of the superconducting and antiferromagnetic subspaces, instead simultaneously containing components from both subspaces and, hence, characterizing regions that are at once partially superconducting and partially antiferromagnetic. In this chapter we examine a simple but potentially interesting property of this model: in antiferromagnetic regions of the phase diagram this model supports three-(spatial)-dimensional antiferromagnetic hedgehog configurations that find it energetically favorable to have superconducting cores, as depicted schematically in Fig. 5.1.

It should be noted that the subject of the present chapter is, loosely speaking, conjugate to that of Ref. [83] in which it is shown that, within the SO(5) approach, the cores of vortices in the superconducting order parameter should not be singular, the mechanism for the evasion of a singularity being escape from the two superconducting dimensions into the three antiferromagnetic ones.

The research presented in this Chapter has been reported in Ref. [85].

5.2 Antiferromagnetic hedgehogs with superconducting cores

What we mean by antiferromagnetic hedgehog configurations with superconducting cores are energetically-stationary spatial configurations of the order parameter $\mathbf{n}(\mathbf{r})$ having the following properties: (i) Far from the (arbitrarily-located) center, the configuration $\mathbf{n}(\mathbf{r})$ closely resembles a (nonsuperconducting) antiferromagnetic hedgehog (i.e., a point defect in which the Néel vector points radially away from the center, or some global SO(3) rotation of this configuration) and the quantity $\sin^2\chi$ $\left[\,\equiv \sum_{a=4}^{5} (n^a)^2\,\right]$, which measures the degree of superconducting order (without regard to its phase), is small. Correspondingly, the complement $\cos^2\chi$ $\left[\,\equiv \sum_{a=1}^{3} (n^a)^2\,\right]$, which measures the degree of antiferromagnetic order without regard to its orientation, is close to unity. (ii) As the center of the configuration is approached, however, the order parameter escapes from dimensions 1, 2 and 3 into dimensions 4 and 5, so that superconducting order is acquired at the expense of antiferromagnetic order. Said equivalently, the angle χ rotates from 0 to $\pi/2$ as the center of the configuration is approached. (In principle, more exotic hedgehog excitations are possible, in which the antiferromagnetic order varies more rapidly. For the sake of simplicity we shall primarily focus on the simplest class.) By this mechanism, the medium is able to remain nonsingular, and evade the (albeit finite) free-energy cost of the spatial gradient in the Néel vector (this gradient diverging as the center of the singular, purely antiferromagnetic, configuration is approached) at the expense of condensing locally into the "wrong" (i.e., superconducting) state. (iii) Whilst not being stable global-energetically—the homogeneous antiferromagnetic configuration of course having a lower free energy—antiferromagnetic hedgehog configurations with superconducting cores do turn out to be energetically favorable, compared with purely antiferromagnetic hedgehogs, as we shall see below, at least when amplitude variations of the order parameter are inhibited. Presumably, such configurations are also *locally* energetically stable [94]. From the physical perspective, then, it would be quite intriguing if local regions of superconductivity were created by "stressing" the antiferromagnetism in regions of the phase diagram in which the stable homogeneous state is not superconducting. Moreover, the topological stability of these textures will tend to hold these "stresses" in place.

In the simplest version of Zhang's approach, the free energy F of a three-dimensional sample in which the order parameter $\mathbf{n}(\mathbf{r})$ varies with position $\mathbf{r}$ is given by

$$F = \int d^3r \left\{ \frac{\rho}{2} \sum_{\nu=1}^{3} \sum_{a=1}^{5} (\partial_\nu n^a)^2 + \frac{g}{2} \sum_{a=4}^{5} (n^a)^2 \right\}, \tag{5.1}$$

where ρ is the appropriate stiffness, ν $(= 1, 2, 3)$ runs through the cartesian spatial coordinates, and spatial anisotropies in the gradient term have been accommodated by coordinate rescalings. By tuning the chemical potential μ relative to its critical value μ_c (e.g., by doping), the parameter g $[\propto (\mu_c^2 - \mu^2)]$ is varied such that one moves from a region in which antiferromagnetic states are favored ($g > 0$) to a region in which superconducting states are favored ($g < 0$). This free energy [which is equal to the free energy (Eq. 4.1) used in Chap. 4 up to an overall constant] is invariant under

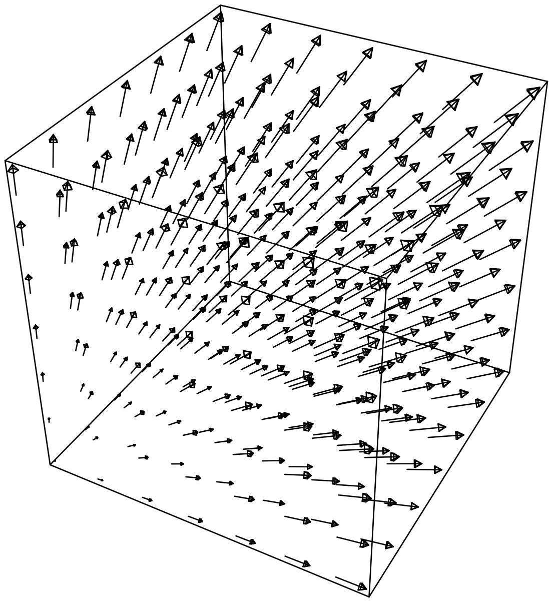

Figure 5.1: An eighth of an antiferromagnetic hedgehog having a superconducting core (determined numerically). The local orientation of the vectors indicates the local orientation of the antiferromagnetism. Their local magnitude indicates the local strength of the antiferromagnetism and, hence, the local weakness of the superconductivity.

separate rotations on the three-dimensional antiferromagnetic and two-dimensional superconducting subspaces; invariance under arbitrary five-dimensional rotations is absent whenever $g \neq 0$. Thus, from any configuration $\mathbf{n}(\mathbf{r})$ one can obtain a configuration having the same free energy via the transformation

$$\mathbf{n} \to \left(R^{\mathrm{A}} \oplus R^{\mathrm{S}}\right) \cdot \mathbf{n}, \tag{5.2}$$

where R^{A} is a (3×3) orthogonal matrix operative in the antiferromagnetic (i.e., $a = 1, 2, 3$) sector (i.e., a magnetization rotation) and R^{S} is a (2×2) orthogonal matrix operative in the superconducting (i.e., $a = 4, 5$) sector (i.e., a phase rotation), and the symbol $\oplus$ indicates that the five-dimensional operator is block-diagonal and composed of one three- and one two-dimensional block.

To calculate the structure of an isolated antiferromagnetic hedgehog with a superconducting core, let us make the hypothesis that components of $\mathbf{n}(\mathbf{r})$ in this configuration can be expressed in the form

$$\begin{pmatrix} n^1 \\ n^2 \\ n^3 \\ n^4 \\ n^5 \end{pmatrix} = \begin{pmatrix} \cos\chi(r)\,\sin\theta\,\cos\phi \\ \cos\chi(r)\,\sin\theta\,\sin\phi \\ \cos\chi(r)\,\cos\theta \\ \sin\chi(r) \\ 0 \end{pmatrix}. \tag{5.3}$$

Here, r, θ and ϕ are spherical polar spatial coordinates centered on the center of the configuration, and the function $\chi(r)$, which allows for interpolation between purely antiferromagnetic and purely superconducting values of the order parameter, is assumed to depend only on the radial distance from the center. This configuration is spherically symmetric, in the sense that for it we have

$$\mathbf{n}(R^{\mathrm{A}} \cdot \mathbf{r}) = \left(R^{\mathrm{A}} \oplus I^{\mathrm{S}}\right) \cdot \mathbf{n}(\mathbf{r}), \tag{5.4}$$

where I^{S} is the identity operation in the superconducting sector. By exchanging the radial variable r for the dimensionless version t (i.e., the radius, measured in units of the correlation length $\xi_\pi \equiv \sqrt{\rho/g}$ for the conversion of antiferromagnetic order into superconducting order) via

$$\begin{aligned} \chi(r) &\equiv X(t), && (5.5) \\ r &\equiv \sqrt{\rho/g}\, t, && (5.6) \end{aligned}$$

and inserting the configuration (5.3) into the free energy (5.1), we find that the free energy is given by

$$F = \tilde{F} \int_0^\tau dt \left\{ \frac{t^2}{2} \dot{X}(t)^2 + \cos^2 X(t) + \frac{t^2}{2} \sin^2 X(t) \right\}, \tag{5.7}$$

where $\tilde{F} \equiv 4\pi g(\rho/g)^{3/2}$, the overdot denotes a derivative with respect to t, and $\sqrt{\rho/g}\,\tau$ is a large-distance cutoff, introduced to render finite the otherwise linearly-divergent free energy. Application of the calculus of variations to the functional F then leads to the stationarity condition

$$t^2\ddot{X} + 2t\dot{X} + \left(1 - \frac{t^2}{2}\right) \sin 2X = 0. \qquad (5.8)$$

The relevant solutions of Eq. (5.8) are: (i) $X(t) \equiv 0$ (i.e., the pure antiferromag-

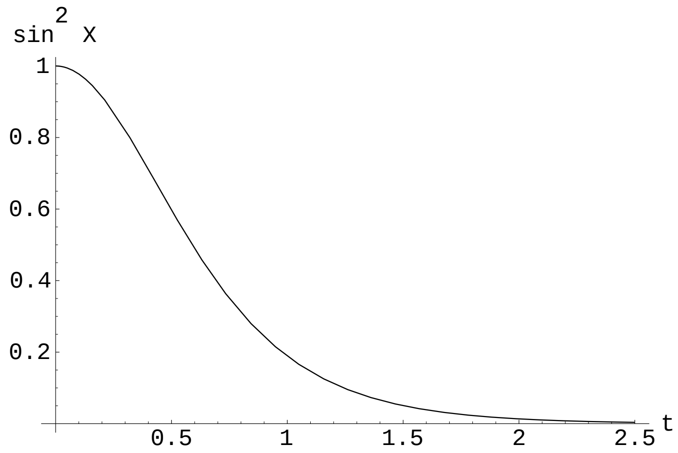

Figure 5.2: The degree of superconductivity $\sin^2 X$ as a function of the scaled radial coordinate t (determined numerically).

netic hedgehog, unescaped into the superconducting directions); and (ii) the solution in which $X(t)$ interpolates between $\pi/2$ and 0 as t varies from 0 to ∞ (i.e., the antiferromagnetic hedgehog with a superconducting core). The precise form of the latter solution is readily found numerically, and is shown in Fig. 5.2. Its asymptotic behavior is $\left(\frac{1}{2}\pi - X\right) \sim t$ (for $t \ll 1$) and $X \sim \exp(-t)$ (for $t \to \infty$). The configuration corresponding to solution (ii) is depicted in Fig. 5.1.

To determine which of the solutions, (i) or (ii), has the lower free energy, let us consider the quantity $\Delta F \equiv \left(F^{(\mathrm{ii})} - F^{(\mathrm{i})}\right)$, where $F^{(\mathrm{i})}$ and $F^{(\mathrm{ii})}$ respectively refer to the free energy of solution (i) and of solution (ii). Then, by using Eq. (5.8), along with integration by parts, we find that

$$\Delta F = \tilde{F} \int_0^\infty dt \left\{ \frac{t^2}{2} - 1 \right\} \Big\{ - X \cos X + \sin X \Big\} \sin X, \qquad (5.9)$$

where convergence at large t permits the replacement of the upper limit by ∞. The numerical evaluation of this quantity gives $\Delta F \approx -0.272\,\tilde{F}$. This indicates that it is energetically favorable for the order parameter in the core of an antiferromagnetic hedgehog to escape into the superconducting directions.

5.3 Consequences of amplitude-sector fluctuations

As we have seen, in the setting of a model in which the amplitude of $\mathbf{n}(\mathbf{r})$ is constrained to be unity, there are hedgehog excitations that have superconducting cores. We now explore the issue of whether such excitations continue to exist in settings in which amplitude variations of $\mathbf{n}(\mathbf{r})$ are inhibited (i.e., are not prohibited, although they are suppressed energetically). Under such circumstances, it is possible—and may prove energetically favorable—for the core of the hedgehog to avoid antiferromagnetic gradient energy via the development of an amplitude-reduced purely-antiferromagnetic core, rather than by escaping into the superconducting directions. To address this issue, we follow Arovas et al. [83] and consider a "soft-spin" generalization of the SO(5) model. Thus we consider a free energy of the form

$$\begin{aligned} F \;=\; \frac{\rho}{2}\int d^3r\; \Big\{ & (\partial_r n(r))^2 + 2r^{-2}\, n(r)^2\, \cos^2\chi(r) \\ & + n(r)^2\, (\partial_r \chi(r))^2 + \xi_\pi^{-2}\, n(r)^2\, \sin^2\chi(r) \Big\} \\ & + a\int d^3r \Big\{ -\frac{1}{2}n(r)^2 + \frac{1}{4}n(r)^4 \Big\}, \end{aligned} \tag{5.10}$$

where $2a$ denotes the squared "mass" associated with the amplitude-sector fluctuations of $\mathbf{n}$, n is the amplitude of $\mathbf{n}$, and we have restricted the discussion to (spatially) spherically symmetric configurations.

In the absence of amplitude fluctuations, the hedgehog with superconducting core has $n \equiv 1$ and χ varying from 0 to $\pi/2$ as the center of the texture is approached. The amplitude-reduced purely antiferromagnetic hedgehog excitation will be one for which n vanishes at the center of the texture and grows to unity at large distances, and $\chi \equiv 0$. The stationarity condition for n, which determines the structure of the amplitude-reduced hedgehog, can be solved numerically, allowing us to obtain the function $n(r)$.

Then, we may insert this back into Eq. (5.10) to obtain the free energy of the purely antiferromagnetic hedgehog with reduced-amplitude core. The free energies of the hedgehog with superconducting core and the purely antiferromagnetic hedgehog with amplitude-reduced core each must be defined with a long distance cutoff to render them finite, but the difference between these two quantities is independent of this cutoff, and turns out to be given by

$$F_{\mathrm{AF}} - F_{\mathrm{SC}} \approx 4\pi\rho \left(0.272\sqrt{\rho/g} - 1.454\sqrt{\rho/a}\right), \tag{5.11}$$

where the subscripts refer to the purely-antiferromagnetic amplitude-reduced (AF) and superconducting-core (SC) hedgehogs. Thus, within the context of this model in which amplitude sector fluctuations are permitted, we find that the hedgehog with superconducting core will be energetically preferred when this quantity is positive, i.e., provided that $g < 0.035a$ [or, equivalently, $\xi_\pi > 5.35\xi_{\mathrm{a}}$, where ξ_{a} ($\equiv \sqrt{\rho/a}$) denotes the fluctuation correlation length for antiferromagnetic fluctuations]. Now, it is typical for ξ_{a} to be on the order of a lattice spacing for the cuprate materials, whereas ξ_π is expected to grow as the superconducting phase boundary is approached from the antiferromagnetic state. Thus, one should anticipate that over a substantial portion of the antiferromagnetic part of the phase diagram, antiferromagnetic hedgehog excitations will have escaped-superconducting (rather than amplitude-reduced purely antiferromagnetic) cores.

5.4 Topological classification of hedgehog excitations

We now turn to the issue of the topological classification of hedgehog excitations having superconducting cores, these excitations being nonsingular textures of the order-parameter field $\mathbf{n}(\mathbf{r})$. In pure antiferromagnets, the existence of singular, hedgehog point-defect excitations is expressed, mathematically, by the statement $\Pi_2(S_2) = Z$ [95, 96]. What this means is that mappings (provided by order-parameter configurations) of spheres in real-space into the antiferromagnetic order-parameter space S_2 fall into homotopically inequivalent classes labeled by the integers (and combine according to integer arithmetic). Within the SO(5) approach, however, the nonsingular hedgehog texture excitations having superconducting cores are described by order parameter configurations $\mathbf{n}(\mathbf{r})$ that lie in the antiferromagnetic subspace S_2 at large distances from the core, but escape into the full order-parameter space S_4, as the core is approached. In order to complete the classification of these textures, then, we should ascertain whether or not there exist homotopically inequivalent textures that, at large distances, are homotopically equivalent and lie in the antiferromagnetic subspace S_2. The appropriate mathematical machinery for this task involves *relative homotopy groups* and *exact homotopy sequences* [96, 97]. To implement this machinery, we consider mappings of cubes (in real-space) such that the surface of the cube is mapped into S_2 whereas the interior of the cube is mapped into S_4. Such mappings are classified according to the relative homotopy group $\Pi_3(S_4, S_2)$. This group is readily computed by making use of the exact sequence of homomorphisms:

$$\Pi_3(S_4) \overset{\beta_3}{\to} \Pi_3(S_4, S_2) \overset{\gamma_3}{\to} \Pi_2(S_2) \overset{\alpha_2}{\to} \Pi_2(S_4). \tag{5.12}$$

Here, β_3, γ_3 and α_2 denote mappings of the elements of the previous group in the sequence to elements of the following group, that, in general, are not isomorphic [98]. Now, as $\Pi_3(S_4)$ and $\Pi_2(S_4)$ are both the trivial group, the homomorphism γ_3 is, in fact, an isomorphism [96, 97], from which it follows that $\Pi_3(S_4, S_2) \cong \Pi_2(S_2) \cong Z$ and, thus, we find that there is no structure in $\Pi_3(S_4, S_2)$ beyond what was already present in $\Pi_2(S_2)$. The physical consequence of this result is that whilst hedgehog excitations fall into homotopically inequivalent classes, the possible nonsingular superconducting cores of a given class of hedgehog are homotopically equivalent to one another.

5.5 Related structures in other condensed states

The notion of the conversion of singularities into textures via the escaping of order-parameters into additional directions has been realized in several other condensed matter settings. For example, (uniaxially) nematic liquid-crystalline media have long been known to exhibit a structure closely related to antiferromagnetic hedgehog configurations with superconducting cores. When confined to a cylinder that imposes homeotropic (i.e., perpendicular) boundary conditions on the nematic alignment, the system can evade the threading of the cylinder by a singularity because the order parameter orientation can escape from the radial plane into the axial direction [99]. This mechanism remains energetically favorable even for diamagnetic nematics in an axial magnetic field (for which escape costs condensation energy).

Superfluid ^{3}He [100] is another system that provides a rich array of topologically interesting textures [101]. The example having the most relevance to the present context is that of hedgehog excitations in ^{3}He-B. The order parameter for ^{3}He-B is a complex-valued 3×3 matrix of the form $A_{\mu\nu} = e^{i\phi} R_{\mu\nu}(\hat{\mathbf{n}}, \theta)$, where ϕ is a phase angle and $R_{\mu\nu}$ is a rotation matrix about the unit vector $\hat{\mathbf{n}}$ by an angle θ. On long length-scales, θ becomes fixed, due to a dipolar coupling, acquiring the value θ_{L}, known as the Leggett angle, so that the low-energy degrees of freedom are expressed by the possible values of ϕ and the directions of $\hat{\mathbf{n}}$. Thus, the order-parameter space G is given by $\mathrm{G} = \mathrm{U}(1) \times S_2$, so that $\Pi_2(\mathrm{G}) = \Pi_2(S_2) = Z$, so that the system may form hedgehogs with the unit vector $\hat{\mathbf{n}}$. On short length-scales, however, θ can vary, so that the order-parameter space is effectively enlarged to $\mathrm{U}(1) \times \mathrm{SO}(3)$. We see that, as $\Pi_2\big(\mathrm{SO}(3)\big) = 0$, over short distances there are no topologically stable point-defects, so that hedgehogs in ^{3}He-B have nonsingular cores.

A similar effect occurs in nematic liquid crystals [102], where on large length-scales the system is uniaxial, so that the relevant order-parameter space is RP_2 (i.e., the real projective plane constructed by identifying opposite points on S_2). On short length-scales, however, the order-parameter space is enlarged to S_4, so that disclinations in the nematic order have nonsingular cores.

5.6 Experimental signatures of hedgehog excitations

We now briefly consider some issues associated with antiferromagnetic hedgehogs having superconducting cores that might be relevant to experiments. These excitations should be present after performing a quench, from high temperature or high magnetic field, into the antiferromagnetic state. The number of excitations per unit volume should be higher for more rapid quenches. As time proceeds after the quench, the number of hedgehog excitations can decrease via their mutual annihilation, although this would require collisions of two or more hedgehogs. Presumably, this process can occur relatively slowly, at least at sufficiently low temperatures, so that one may anticipate regimes in which these excitations, once created, remain long enough for their consequences to be detected.

What experimental signatures might antiferromagnetic hedgehogs with superconducting cores yield? Let us suppose that a sufficiently high density of such excitations can be created, and that this density can be maintained for a sufficiently long time. Then one may crudely regard the excitations as providing a set of randomly located, randomly phased, superconducting inclusions [103]. These inclusions would not be unlike Aslamazov-Larkin paraconducting fluctuations [104], except that they would be "externally" maintained and, therefore, could be much longer lived. One might hope that these inclusions would be detectable in electrical conductivity experiments, their presence leading to an enhancement of the conductivity. (One would need to account for scattering from the antiferromagnetic hedgehogs which, presumably, diminishes the conductivity.) This enhancement should be suppressed by magnetic fields, and by the decay of the excitations. Similarly, one might also envisage observing Andreev reflection from the superconducting inclusions (although capacitive charging effects may suppress this effect[105]).

An externally applied magnetic field will be partially screened by these inclusions, leading to a negative contribution to the magnetic susceptibility. To estimate the size of this effect, we approximate the hedgehog cores to be uniformly superconducting and spherical in shape [106]. In the regime where the London penetration depth λ is much longer than the core radius ξ, this leads to a diamagnetic susceptibility contribution $\chi = -\delta\xi^5/40\pi\lambda^2$, where δ is the number of excitations per unit volume. One might also hope that the presence of antiferromagnetic hedgehogs with superconducting cores would be detectable via probes such as nuclear magnetic resonance, electromagnetic absorption and hedgehog/antihedgehog pair creation and, perhaps fancifully, scanning tunneling microscopy (e.g., with a magnetic tip).

In addition, these excitations should leave their fingerprint on the (staggered) magnetic structure factor $S(k)$, this factor being determined by $\mathbf{N}(\mathbf{k})$ (i.e., the Fourier transform of the antiferromagnetic Néel vector at the probing wave vector $\mathbf{k}$) via

$$S(k) \equiv V^{-1}\,\mathbf{N}(\mathbf{k})\cdot\mathbf{N}(\mathbf{k}), \tag{5.13}$$

where V is the volume of the system. Specifically, for length scales that are long compared with the core size ξ_π but short compared to the spacing between the hedgehogs $\delta^{-1/3}$, we expect $S(k)$ to have the conventional hedgehog form. However, for length scales that are short compared with the core size but long compared with the lattice spacing, we expect a reduction in $S(k)$ (and hence scattering), owing to the diminution of the Fourier amplitude of the antiferromagnetic moment at these scales. The computed hedgehog structure does indeed realize this scenario:

$$S(k) \sim \begin{cases} \delta\,\xi^6\,(k\xi)^{-6} & \text{for } \delta^{-1/3} \ll k \ll \xi_\pi^{-1}; \\ \delta\,\xi^6\,(k\xi)^{-10} & \text{for } \xi_\pi^{-1} \ll k. \end{cases} \tag{5.14}$$

However, it should be noted that, being sensitive only to antiferromagnetic order, this particular probe does not directly ascertain whether or not the cores of hedgehog excitations are superconducting (except via the dependence of the size of the cores on the location of the system in the phase diagram).

5.7 Concluding remarks

If detected in experiments, antiferromagnetic hedgehogs with superconducting cores would provide striking evidence in support of Zhang's SO(5) approach to the physics of high-temperature superconducting materials. Their presence would corroborate the notion that superconducting excitations are essential low-energy excitations of the antiferromagnetic state. Moreover, it would prove rather intriguing to have at hand a physical system in which superconductivity is induced by the distortion of a thermodynamically preferred nonsuperconducting state.

Appendix A

Single particle Green function

Our aim is to obtain Eq. (2.1) for the one-fermion Green function in the presence of a fluctuating pair potential. We begin by expressing the partition function for our system as a fermionic path integral:

$$\begin{aligned} Z &\propto \int D\psi_\uparrow^\dagger D\psi_\uparrow D\psi_\downarrow^\dagger D\psi_\downarrow \exp(-S_\psi), & \text{(A.1)} \\ S_\psi &\equiv \sum_{\sigma=\uparrow,\downarrow} \int d^2r \int_0^\beta d\tau\, \psi_\sigma^\dagger(\partial_\tau + \hat{h})\psi_\sigma & \text{(A.2)} \\ &+ \int d^2r\, d^2r' \int_0^\beta d\tau\, \psi_\uparrow^\dagger(\mathbf{r},\tau)\psi_\downarrow^\dagger(\mathbf{r}',\tau)\psi_\downarrow(\mathbf{r}',\tau)\psi_\uparrow(\mathbf{r},\tau)U(\mathbf{r},\mathbf{r}'), \\ \hat{h} &\equiv -\nabla^2 - k_{\mathrm{F}}^2 + V(\mathbf{r}). & \text{(A.3)} \end{aligned}$$

Here, $\psi_\uparrow(\mathbf{r},\tau)$ and $\psi_\downarrow(\mathbf{r},\tau)$ are fermion fields and $\hat{h}$ is the single-particle Hamiltonian in the presence of an impurity potential $V(\mathbf{r})$. The attractive fermionic pairing interaction is given by $U(\mathbf{r},\mathbf{r}')$ (and has been chosen to be instantaneous in time, for simplicity). We use a system of units in which $\hbar^2/2m = 1$ (where m is the effective fermion mass) and Boltzmann's constant $k_{\mathrm{B}} = 1$. The chemical potential for our system is given by k_{F}^2, where k_{F} is the Fermi wavevector. Following the presentation in Kleinert [43], we decouple the pairing term using a Hubbard-Stratonovich transformation involving the pairing field $\Delta(\mathbf{r},\mathbf{r}';\tau)$ to obtain

$$\begin{aligned}
Z &\propto \int Df^\dagger Df D\Delta^\dagger D\Delta \exp(-S_f), && \text{(A.4)}\\
S_f &\equiv \int d^2r\, d^2r' d\tau \left(f^\dagger(\mathbf{r},\tau) A(\mathbf{r},\mathbf{r}';\tau) f(\mathbf{r}',\tau) - \int d^2r d^2r' d\tau \frac{|\Delta(\mathbf{r},\mathbf{r}';\tau)|^2}{U(\mathbf{r},\mathbf{r}')} \right), \\
A(\mathbf{r},\mathbf{r}';\tau) &\equiv \begin{pmatrix} \partial_\tau + \hat{h} & 0 \\ 0 & \partial_\tau - \hat{h} \end{pmatrix} \delta(\mathbf{r}-\mathbf{r}') + \begin{pmatrix} 0 & \Delta(\mathbf{r},\mathbf{r}';\tau) \\ \Delta^\dagger(\mathbf{r},\mathbf{r}';\tau) & 0 \end{pmatrix},
\end{aligned}$$

where $\Delta^\dagger(\mathbf{r},\mathbf{r}';\tau) \equiv (\Delta(\mathbf{r}',\mathbf{r};\tau))^*$. Here, we have expressed the fermions in terms of Nambu spinors

$$f(\mathbf{r},\tau) \equiv \begin{pmatrix} \psi_\uparrow(\mathbf{r},\tau) \\ \psi_\downarrow^\dagger(\mathbf{r},\tau) \end{pmatrix}. \tag{A.5}$$

The one-fermion Green function is given by

$$\mathcal{G}(x,x') = -\begin{pmatrix} \langle T_\tau \psi_\uparrow(x) \psi_\uparrow^\dagger(x')\rangle & \langle T_\tau \psi_\uparrow(x) \psi_\downarrow(x')\rangle \\ \langle T_\tau \psi_\downarrow^\dagger(x) \psi_\uparrow^\dagger(x')\rangle & \langle T_\tau \psi_\downarrow^\dagger(x) \psi_\downarrow(x')\rangle \end{pmatrix}, \tag{A.6}$$

where $x \equiv (\mathbf{r},\tau)$, the angle brackets represent the thermodynamic average associated with the partition function in Eq. (A.1), and T_τ is the time-ordering operator. It is convenient to express $\mathcal{G}(x,x')$ in terms of a generating functional $Z[j,j^\dagger]$:

$$\begin{aligned}
\mathcal{G}(x,x') &= -\frac{1}{Z} \frac{\delta^2 Z}{\delta j^\dagger(x) \delta j(x')}\bigg|_{j^\dagger=j=0}, && \text{(A.7)}\\
Z[j,j^\dagger] &\propto \int Df^\dagger Df D\Delta^\dagger D\Delta \exp(-S_j), && \text{(A.8)}\\
S_j &\equiv S_f + \int dx \left(f^\dagger(x) j(x) + j^\dagger(x) f(x) \right), && \text{(A.9)}
\end{aligned}$$

where j and $j^\dagger$ are source fields. By evaluating the functional integral over the fields f and $f^\dagger$, and performing the functional derivatives indicated in Eq. (A.7), we arrive at the following expression for $\mathcal{G}$:

$$\begin{aligned}
\mathcal{G}(x,x') &= \frac{\int D\Delta^\dagger D\Delta \, \mathrm{e}^{-S[\Delta]} \, G(x,x';\Delta)}{\int D\Delta^\dagger D\Delta \, \mathrm{e}^{-S[\Delta]}}, && \text{(A.10)}\\
S[\Delta] &\equiv -\mathrm{Tr} \ln[A] - \int d^2r\, d^2r' d\tau \frac{|\Delta(\mathbf{r},\mathbf{r}';\tau)|^2}{U(\mathbf{r},\mathbf{r}')}, && \text{(A.11)}
\end{aligned}$$

where $G(x, x'; \Delta)$ is given by Eq. (2.2). Although the phase-fluctuation action is, in principle, obtained from Eq. (A.11), in Chapter 2 we shall simply assume a phenomenological form for $S[\Delta]$.

Appendix B

Semiclassical approximation to the density of states

In this Appendix we present an alternative derivation of Eq. (2.24). In particular, our aim is to examine in detail the relationship between the Bogoliubov–de Gennes Green function and the one-dimensional Andreev Green function. Our calculations will follow Waxman and Ivanova-Moser [107]. For simplicity, we focus on the case of a pure d-wave superconductor [i.e. no phase fluctuations, and the pair potential $\Delta = \Delta(\mathbf{p})$]. The density of states (DOS) is given by

$$\rho(E) = -\pi^{-1} \mathrm{Im}\,\mathrm{Tr} \int d^2r\, \langle \mathbf{r} | \frac{1}{E - H_{\mathrm{BdG}}(\mathbf{p}, \mathbf{r})} | \mathbf{r} \rangle, \tag{B.1}$$

where

$$H_{\mathrm{BdG}}(\mathbf{p}, \mathbf{r}) \equiv \begin{pmatrix} p^2 - k_{\mathrm{F}}^2 + V(\mathbf{r}) & \Delta \\ \Delta & -p^2 + k_{\mathrm{F}}^2 - V(\mathbf{r}) \end{pmatrix}, \tag{B.2}$$

and E is understood to have a small positive imaginary part (i.e. $E \to E + i\delta$). Here, $\mathbf{p}$ is the operator $\mathbf{p} = -i\boldsymbol{\nabla}$. The next step is to use the identity [107]

$$\int d^d r\, \langle r | f(\mathbf{p}, \mathbf{r}) | r \rangle = \int \frac{d^d r\, d^d k}{2\pi}\, f(\mathbf{k} - i\boldsymbol{\nabla}, \mathbf{r}). \tag{B.3}$$

In the present case, this identity (for $d = 2$) leads to the following expression for $\rho(E)$:

$$\rho(E) = -\pi^{-1}\mathrm{Im}\,\mathrm{Tr}\int \frac{d^2r\,d^2k}{(2\pi)^2}\frac{1}{E - H_{\mathrm{BdG}}(\mathbf{k} - i\boldsymbol{\nabla}, \mathbf{x})}. \tag{B.4}$$

Next, we expand the quantity $(\mathbf{k} - i\boldsymbol{\nabla})$ to lowest order in derivatives, i.e., $(\mathbf{k} - i\boldsymbol{\nabla}) \approx k^2 - 2i\mathbf{k}\cdot\boldsymbol{\nabla}$. In addition, we approximate $\Delta(\mathbf{k} - i\boldsymbol{\nabla}) \simeq \Delta(\mathbf{k})$. Then, we have

$$\rho(E) = -\pi^{-1}\mathrm{Im}\,\mathrm{Tr}\int d^2r \int \frac{d^2k}{(2\pi)^2}\frac{1}{E - H_1}\,, \tag{B.5}$$

$$H_1 \equiv \begin{pmatrix} k^2 - 2i\mathbf{k}\cdot\boldsymbol{\nabla} - k_{\mathrm{F}}^2 + V(\mathbf{r}) & \Delta(\mathbf{k}) \\ \Delta(\mathbf{k}) & -k^2 + 2i\mathbf{k}\cdot\boldsymbol{\nabla} + k_{\mathrm{F}}^2 - V(\mathbf{r}) \end{pmatrix}. \tag{B.6}$$

The semiclassical approximation amounts to assuming that the integral over $\mathbf{k}$ is dominated by terms for which $\mathbf{k} \simeq k_{\mathrm{F}}\dot{\mathbf{x}}_{\mathrm{c}}(s)$. Here, $\mathbf{x}_{\mathrm{c}}(s)$ is a classical scattering trajectory passing through the point $\mathbf{r}$ at s satisfying Newton's equation

$$k_{\mathrm{F}}^2\,\partial_s^2\mathbf{x}_{\mathrm{c}}(s) = -\boldsymbol{\nabla}V(\mathbf{x}_{\mathrm{c}}(s)), \tag{B.7}$$

as well as the energy conservation condition

$$k_{\mathrm{F}}^2|\dot{x}_{\mathrm{c}}(s)|^2 + V = k_{\mathrm{F}}^2. \tag{B.8}$$

At each real space position $\mathbf{r}$, there are an entire manifold of such classical trajectories associated with various directions $\mathbf{n}$. For each $\mathbf{n}$, then, we define $\mathbf{k} = k_{\mathrm{F}}\dot{\mathbf{x}}_{\mathrm{c}}(s) + \mathbf{q}$ where $\mathbf{q}$ points in the $\mathbf{n}$ direction:

$$\rho(E) = -\pi^{-1}\mathrm{Im}\,\mathrm{Tr}\int d^2r \int \frac{d\mathbf{n}}{2\pi}\frac{q\,dq}{2\pi}\frac{1}{E - H_2}\,, \tag{B.9}$$

$$H_2 \equiv \begin{pmatrix} q^2 - 2ik_{\mathrm{F}}\dot{\mathbf{x}}_{\mathrm{c}}(s)\cdot\boldsymbol{\nabla} & \Delta(\dot{\mathbf{x}}_{\mathrm{c}}(s)) \\ \Delta(\dot{\mathbf{x}}_{\mathrm{c}}(s)) & -q^2 + 2ik_{\mathrm{F}}\dot{\mathbf{x}}_{\mathrm{c}}(s)\cdot\boldsymbol{\nabla} \end{pmatrix},$$

where we have made use of Eq. (B.8) At this point, we are summing over all trajectories passing through a given point $\mathbf{r}$, then integrating over $\mathbf{r}$. Equivalently, we can perform the spatial integral along a given trajectory, then sum over all trajectories (labeled by an impact parameter b for a given incoming momentum direction

$\mathbf{n}$). This amounts (for a given $\mathbf{n}$) to changing variables from $\mathbf{r}$ to s and b. Taking the Jacobian for this variable change to be 1 [108], and using the chain rule formula $\partial_s g(\mathbf{x}_c(s)) = \dot{\mathbf{x}}_c(s)\cdot\boldsymbol{\nabla} g$ as well as Eq. (B.8) we obtain

$$\begin{aligned}
\rho(E) &= -\pi^{-1}\mathrm{Im}\,\mathrm{Tr}\int\frac{d\mathbf{n}}{2\pi}\int db\,ds\int\frac{q\,dq}{2\pi}\frac{1}{E-H_3}\,, \\
H_3 &\equiv \begin{pmatrix} q^2-2ik_\mathrm{F}\partial_s & \Delta(\dot{\mathbf{x}}_c(s)) \\ \Delta(\dot{\mathbf{x}}_c(s)) & -q^2+2ik_\mathrm{F}\partial_s \end{pmatrix}.
\end{aligned} \tag{B.10}$$

Next, we make a change of variables from q to $k \equiv q^2/2k_\mathrm{F}$. Then, we have

$$\rho(E) = -\pi^{-1}\mathrm{Im}\,\mathrm{Tr}\int\frac{d\mathbf{n}}{2\pi}\int db\,ds\,k_\mathrm{F}\int\frac{dk}{2\pi}\frac{1}{E-H_4}\,, \tag{B.11}$$

$$H_4 \equiv \begin{pmatrix} 2k_\mathrm{F}k-2ik_\mathrm{F}\partial_s & \Delta(k_\mathrm{F}\dot{\mathbf{x}}_c(s)) \\ \Delta(k_\mathrm{F}\dot{\mathbf{x}}_c(s)) & -2k_\mathrm{F}k+2ik_\mathrm{F}\partial_s \end{pmatrix}. \tag{B.12}$$

The utility of this variable change is that now we are in a position to again use Eq. (B.3), but now in the reverse direction and with $d = 1$. Then, we finally obtain

$$\rho(E) = -\pi^{-1}\mathrm{Im}\,\mathrm{Tr}\int\frac{d\mathbf{n}}{2\pi}\,k_\mathrm{F}\int db\,ds\langle s|\frac{1}{E-H_\mathrm{A}}|s\rangle, \tag{B.13}$$

$$H_\mathrm{A} \equiv \begin{pmatrix} -2ik_\mathrm{F}\partial_s & \Delta(k_\mathrm{F}\dot{\mathbf{x}}_c(s)) \\ \Delta(k_\mathrm{F}\dot{\mathbf{x}}_c(s)) & 2ik_\mathrm{F}\partial_s \end{pmatrix}, \tag{B.14}$$

where H_A is the Andreev Hamiltonian. This expression gives us a precise relationship between $\rho(E)$ and the Green function of H_A (i.e. $\langle s|(E-H_\mathrm{A})^{-1}|s'\rangle$) associated with a particular trajectory. This Green function may be expressed in terms of the normalized eigenstates ψ_n of H_A as

$$\langle s|(E-H_\mathrm{A})^{-1}|s'\rangle = \sum_n \frac{\psi_n(s)\;\psi_n^\dagger(s')}{E-E_n}. \tag{B.15}$$

The DOS, then, is given by inserting this into Eq. (B.13) and making use of the small imaginary part of E, leading to

$$\rho(E) = k_\mathrm{F}\int\frac{d\mathbf{n}}{2\pi}\int db\sum_n\delta(E-E_n(\mathbf{n},b)),. \tag{B.16}$$

where in this last equation we have explicitly indicated the dependence of E_n on $\mathbf{n}$ and b. Equation (2.24), then, amounts to keeping only the lowest order term in this sum, which is due to the perturbed zero-energy state.

Appendix C

Calculation of the tunneling current

The purpose of this Appendix is to derive Eq. (3.4) for the fourth-order contribution to the tunneling current. The total Hamiltonian for our system consists of the Hamiltonians for the two sides (H_{N} and H_{P}), together with the tunneling Hamiltonian H_{T}:

$$H_{\mathrm{T}} \equiv \sum_{\sigma=\pm} \int_{\mathrm{P}} d^3r \int_{\mathrm{N}} d^3s \left(t_{\mathbf{r},\mathbf{s}}\, d^{\dagger}_{\mathbf{r},\sigma}\, c_{\mathbf{s},\sigma} + t^{*}_{\mathbf{r},\mathbf{s}}\, c^{\dagger}_{\mathbf{s},\sigma}\, d_{\mathbf{r},\sigma} \right). \tag{C.1}$$

The quantum-mechanical current operator $\hat{I}$ is obtained from the Heisenberg equation of motion for the number operator on the N side. That is,

$$\hat{I} = e\dot{N}_N = e\frac{i}{\hbar}[H, N_N], \tag{C.2}$$

where N_N is the number operator on the normal side of the interface, and which commutes with the Hamiltonian for the normal side. In terms of $\hat{I}$, the physical current $I(V)$ is given by

$$I(V) = \mathrm{Tr}\, \mathrm{e}^{-\beta H} \hat{I}, \tag{C.3}$$

$$\hat{I} = \frac{2e}{\hbar} \sum_{\sigma} \int_{\mathrm{P}} d^3r \int_{\mathrm{N}} d^3s \, \mathrm{Im} \left(t_{\mathbf{r},\mathbf{s}} e^{iHt/\hbar} d^{\dagger}_{\mathbf{r},\sigma} c_{\mathbf{s},\sigma} e^{-iHt/\hbar} \right), \tag{C.4}$$

where voltage difference V across the junction enters via the chemical potential difference between the normal and superconducting sides:

$$eV = \mu_{\rm N} - \mu_{\rm P}. \tag{C.5}$$

We calculate I by first analytically continuing the time $t \to -i\hbar\tau$ and then calculating the corresponding Matsubara tunneling current $\tilde{I}$. This quantity takes the form

$$\tilde{I} = \frac{2e}{\hbar}\sum_{\sigma}\int_{\rm P} d^3r \int_{\rm N} d^3s \,{\rm Im}\left\langle T_\tau \left(t_{\mathbf{r},\mathbf{s}}\, {\rm e}^{H_0\tau/\hbar} d^\dagger_{\mathbf{r},\sigma}\, c_{\mathbf{s},\sigma} {\rm e}^{-H_0\tau/\hbar} U(\beta)\right)\right\rangle \tag{C.6}$$

$$U(\beta) = T_\tau \exp\left[-\int_0^\beta d\tau\, e^{H_0\tau/\hbar}\, H_{\rm T}\, e^{-H_0\tau/\hbar}\right], \tag{C.7}$$

where $H_0 \equiv H_{\rm N} + H_{\rm P}$ and T_τ is the time-ordering operator. The interaction picture expression for quantities like $d^\dagger_{\mathbf{r},\sigma}\, c_{\mathbf{s},\sigma}$ is given by

$${\rm e}^{H_0\tau/\hbar} d^\dagger_{\mathbf{r},\sigma}\, c_{\mathbf{s},\sigma}, {\rm e}^{-H_0\tau/\hbar} = d^\dagger_{\mathbf{r},\sigma}(\tau)\, c_{\mathbf{s},\sigma}(\tau) {\rm e}^{-i\Omega\tau}, \tag{C.8}$$

where

$$c_{\mathbf{r},\sigma}(\tau) \;\equiv\; {\rm e}^{K_0\tau} c_{\mathbf{r},\sigma} {\rm e}^{-K_0\tau}, \tag{C.9}$$

$$K_0 \;\equiv\; H_0 - \mu_{\rm N} N_{\rm N} - \mu_{\rm P} N_{\rm P}, \tag{C.10}$$

(and similarly for $d_{\mathbf{r},\sigma}(\tau)$) and $i\Omega$ is a bosonic Matsubara frequency (i.e., $i\Omega = 2n\pi T$ for n integral) which must be analytically continued via $i\Omega \to eV$ at the end of the calculation to obtain I.

Similarly, the interaction picture expression for $H_{\rm T}$ is given by

$$\begin{aligned} &e^{H_0\tau/\hbar}\, H_{\rm T}\, e^{-H_0\tau/\hbar} \\ &= \sum_\sigma \int_{\rm P} d^3r \int_{\rm N} d^3s \left(t_{\mathbf{r},\mathbf{s}}\, d^\dagger_{\mathbf{r},\sigma}(\tau)\, c_{\mathbf{s},\sigma}(\tau)\, e^{-i\Omega\tau} + t^*_{\mathbf{r},\mathbf{s}}\, c^\dagger_{\mathbf{s},\sigma}(\tau)\, d_{\mathbf{r},\sigma}(\tau)\, e^{i\Omega\tau}\right) \times e^{-i\omega_\delta\tau}, \end{aligned} \tag{C.11}$$

where we have included the factor $e^{-i\omega_\delta\tau}$ so that (upon performing the analytic continuations $-i\hbar\tau \to t$ and $i\omega_\delta \to i\delta$) Eq. (C.11) vanishes in the distant past. Physically, this implements the notion that, for $t \to -\infty$, $H_{\mathrm{T}} = 0$ (and the N and P sides are separately in equilibrium). Throughout our calculation, we take frequencies such as ω_δ and Ω to be bosonic Matsubara frequencies. The physical current I is then obtained by making the appropriate analytic continuations (i.e. $i\Omega \to eV$, $i\omega_\delta \to i\delta$ and $-i\hbar\tau \to t$) As noted in the main text [immediately preceding Eq. (3.4)], our primary interest is in the phase-sensitive contribution to I associated with four powers of the tunneling matrix element. To obtain this, we expand $U(\beta)$ to third order, obtaining

$$
\begin{aligned}
&\left\langle T_\tau \left(t_{\mathbf{r},\mathbf{s}}\, d^\dagger_{\mathbf{r},\sigma}(\tau)\, c_{\mathbf{s},\sigma}\, e^{-i\Omega\tau}\, U(\beta)\right)\right\rangle|_{\text{third}} \\
&= -\frac{3}{3!}\int_{\langle\text{coord's}\rangle} t_{\mathbf{r},\mathbf{s}}\, t^*_{\mathbf{r_1},\mathbf{s_1}}\, t^*_{\mathbf{r_3},\mathbf{s_3}}\, t_{\mathbf{r_4},\mathbf{s_4}} \int d\tau_2\, d\tau_3\, d\tau_4 \\
&\qquad \times \left\langle d^\dagger_{\mathbf{r},\sigma}(\tau)\, d^\dagger_{\mathbf{r_1},\sigma_1}(\tau_2)\, d_{\mathbf{r_3},\sigma_3}(\tau_3)\, d_{\mathbf{r_4},\sigma_4}(\tau_4)\right\rangle \\
&\qquad \times \left\langle c_{\mathbf{s},\sigma}(\tau)\, c_{\mathbf{s_1},\sigma_1}(\tau_2)\, c^\dagger_{\mathbf{s_3},\sigma_3}(\tau_3)\, c^\dagger_{\mathbf{s_4},\sigma_4}(\tau_4)\right\rangle \\
&\qquad \times \exp[-i\Omega(\tau+\tau_2-\tau_3-\tau_4)]\, \exp[-i\omega_\delta(\tau_2+\tau_3+\tau_4)]
\end{aligned}
\tag{C.12}
$$

By inserting this into Eq. (C.6) (and using our expression for $t_{\mathbf{r},\mathbf{s}}$ as noted in the main text), we obtain Eq. (3.4) for $\tilde{I}$.

References

[1] J. G. Bednorz and K. A. Müller, Z. Phys. **64**, 189 (1986).

[2] J. Bardeen, L. N. Cooper and J. R. Schrieffer, Phys. Ref **108** 1175 (1957).

[3] D. A. Wollman, D. J. Van Harlingen, W. C. Lee, D. M. Ginsberg and A. J. Leggett, Phys. Rev. Lett **71**, 2134 (1994).

[4] W. W. Warren Jr., R. E. Walstedt, R. F. Bell, R. J. Cava, G. P. Espinoza, L. F. Schneemeyer and J. V. Waszczak, Phys. Rev. Lett. **62**, 1193 (1989).

[5] A. Gupta and K.-W. Ng, Phys. Rev. B **58**, 8901 (1998).

[6] Ch. Renner, B. Revaz, J.-Y. Genoud, K. Kadowaki and Ø. Fischer, Phys. Rev. Lett. **80**, 149 (1998).

[7] M. R. Norman, H. Ding, M. Randeria, J. C. Campuzano, T. Yokoya, T. Takeuchi, T. Takahashi, T. Mochiku, K. Kadowaki, P. Guptasarma and D. G. Hinks, Nature **392**, 157 (1998).

[8] Among these are SO(5) [9], SU(2) slave boson [10], pre-formed pairs [11], antiferromagnetic spin fluctuations [12], and d-density wave [13], to give a non-exhaustive list.

[9] S.-C. Zhang, Science **275**, 1089 (1997).

[10] X.-G. Wen and P. A. Lee, Phys. Rev. Lett. **76**, 503 (1996).

[11] J. Maly, K. Levin and D. Z. Liu, Phys. Rev. B **54**, R15657 (1996); B. Jankó, J. Maly and K. Levin, Phys. Rev. B **56**, R11407 (1997).

[12] J. Schmalian, D. Pines and B. Stojkovic, Phys. Rev. Lett. **80**, 3839 (1998).

[13] S. Chakravarty, R. B. Laughlin, D. K. Morr and C. Nayak, **64**, 094503 (2001).

[14] V. Emery and S. A. Kivelson, Nature (London) **374**, 434 (1995).

[15] M. Franz and A. J. Millis, Phys. Rev. B **58**, 14572 (1998).

[16] H.-J. Kwon and A. T. Dorsey, Phys. Rev. B **59**, 6438 (1999).

[17] V. M. Loktev, R. M. Quick and S. Sharapov, cond-mat/0012082, "Phase Fluctuations and Pseudogap Phenomena".

[18] Z. A. Xu, N. P. Ong, Y. Wang, T. Kakeshita and S. Uchida, Nature (London) **406**, 486 (2000).

[19] J. Corson, R. Mallozzi, J. Orenstein, J. N. Eckstein and I. Bozovic, Nature (London) **398**, 221 (1999).

[20] V. Ambegaokar, B. I. Halperin, D. R. Nelson and E. D. Siggia, Phys. Rev. B **20**, 1806 (1980).

[21] A. G. Loeser, Z.-X. Shen, D. S. Dessau, D. S. Marshall, C. H. Park, P. Fournier and A. Kapitulnik, Science **273**, 325 (1996).

[22] H. Ding, T. Yokoya, J. C. Campuzano, T. Takahashi, M. Randeria, M. R. Norman, T. Mochiku, K. Kadowaki and J. Giapintzakis, Nature (London) **382**, 51 (1996).

[23] H.-Y. Choi, Y. Bang and D. K. Campbell, Phys. Rev. B **61**, 9748 (2000).

[24] B. Jankó, I. Kosztin, K. Levin, M. R. Norman and D. J. Scalapino, Phys. Rev. Lett. **82**, 4304 (1999).

[25] D. E. Sheehy, P. M. Goldbart, J. Schmalian and A. Yazdani, Phys. Rev. B **62**, 4105 (2000).

[26] I. Martin and A. Balatsky, Phys. Rev. B **62**, R6124 (2000).

[27] By extended impurities we mean impurities with a spatial extent that is large compared to the Fermi wavelength λ_{F}.

[28] C.-R. Hu, Phys. Rev. Lett. **72**, 1526 (1994).

[29] L. J. Buchholtz, M. Palumbo, D. Rainer and J. A. Sauls, J. Low Temp. Phys. **101**, 1079 (1995); ibid. **101**, 1099 (1995).

[30] M. Fogelström, D. Rainer and J. A. Sauls, Phys. Rev. Lett. **79**, 281 (1997).

[31] In the context of scattering due to point-like impurities [32], the density of states possesses low-energy resonances, the energies of which move to zero energy as the strength of the impurity potential is increased.

[32] A. V. Balatsky, M. I. Salkola and A. Rosengren, Phys. Rev. B **51**, 15547 (1995); M. I. Salkola, A. V. Balatsky and D. J. Scalapino, Phys. Rev. Lett. **77**, 1841 (1996).

[33] M. Covington, R. Scheuerer, K. Bloom and L. H. Greene, Appl. Phys. Lett. **68** 1717 (1996); M. Covington, M. Aprili, E. Paraoanu, L. H. Greene, F. Xu, J. Zhu and C. A. Mirkin, Phys. Rev. Lett. **79**, 277 (1997).

[34] A. Yazdani, C. M. Howald, C. P. Lutz, A. Kapitulnik and D. M. Eigler, Phys. Rev. Lett. **83** (1999) 176.

[35] E. Hudson, S. H. Pan, A. K. Gupta, K.-W. Ng and J. C. Davis, Science **285**, 88 (1999).

[36] I. Adagideli, P. M. Goldbart, A. Shnirman and A. Yazdani, Phys. Rev. Lett. **83**, 5571 (1999).

[37] The analysis of low-energy quasiparticle states reported in Ref. [36] is based on an application of Witten's supersymmetric quantum mechanics [38, 39].

[38] E. Witten, Nucl. Phys. **B 188** (1981) 513.

[39] For an introduction to supersymmetric quantum mechanics, see, e.g., G. Junker, *Supersymmetric Methods in Quantum and Statistical Physics* (Springer, Berlin, 1996).

[40] H. V. Kruis, I. Martin and A. V. Balatsky cond-mat/0008349, "Impurity induced resonant state in a pseudogap state of a high temperature superconductor".

[41] Among the virtues of the setting of extended (rather than point-like) impurities are: (i) the robustness of the low-energy states, by which we mean the insensistivity of their energies to spatial variations in the modulus of the d-wave pair-potential; and (ii) the presence of low-energy states are signatures of superconductivity, specifically with sign changes in the pair-potential.

[42] D. E. Sheehy, I. Adagideli, P. M. Goldbart and A. Yazdani, cond-mat/0106026, "Probing d-wave pairing correlations in the pseudogap regime of the cuprate superconductors via low-energy states near impurities".

[43] H. Kleinert, Fortschr. Phys. **26**, 565 (1978).

[44] Although $\Delta_0(\mathbf{k}, \mathbf{R})$ is expected to be independent of $\mathbf{R}$ away from the impurity

(i.e. in the bulk), near the impurity pair-breaking processed may suppress the pair-potential amplitude leading to $\mathbf{R}$ dependence.

[45] Note that we are ignoring broader classes of fluctuations, such as those that would take $\bar{\Delta}(\mathbf{k}, \mathbf{R})$ out of the space of $\mathrm{d}_{x^2-y^2}$ states. For example, one can envision the situation in which phase-fluctuating d-wave order is augmented by fluctuating local s-wave order. Additional classes of fluctuations, such as this, can readily be incorporated in the present scheme, and would lead to further broadening of the single-particle spectral function.

[46] A. F. Andreev, Zh. Eksp. Teor. Fiz. **46**, 1823 (1964) [Sov. Phys. JETP **19**, 1228 (1964)].

[47] The caveat with regard to our focusing on scatterers that create trajectories having at most one sign change in the pair-potential is meant to eliminate from consideration various very low-energy states associated with trajectories involving an even number of multiple sign-changes of the pair-potential. In particular, we have in mind the following scenario: Imagine a system consisting of two extended impurities. In such a system, there exist trajectories that scatter twice, once from each impurity. Among these, of particular interest are the trajectories that encounter two sign changes, e.g., one can imagine a trajectory that scatters off the first impurity from the positive lobe of the d-wave order parameter to the negative lobe and then off the second impurity from the negative lobe back to the positive lobe. As such a trajectory has no net sign change there will be no zero-energy state. If, however, the impurities are far apart, one can imagine that the supersymmetry analysis applied to each state *individually* (i.e. ignoring the other impurity, and thus giving a zero-energy state for each) would be correct, up to an exponentially small tunneling correction, indicating that such

a doubly-scattering trajectory would provide two states, both very close indeed to zero energy.

[48] Of course, this exponential decay breaks down for trajectories in which at least one of the aympototic directions (incoming or outgoing) tends to a nodal direction. Such trajectories comprise a relatively small fraction of the trajectories and will, henceforth, be neglected.

[49] L. Berezinskiĭ, Zh. Eksp. Teor. Fiz **59**, 907 (1970) [Sov. Phys. JETP **32**, 493-500 (1971)].

[50] For a discussion of the XY-model see, e.g., P. M. Chaikin and T. C. Lubensky, *Principles of Condensed Matter Physics* (Cambridge University Press, 1995), especially Chapter 9.

[51] J. M. Kosterlitz and D. J. Thouless, J. Phys. C **6**, 1181 (1973).

[52] For a discussion of phase-fluctuation models in d-wave superconductors see, e.g., Ref. [53].

[53] A. Paramekanti, M. Randeria, T. V. Ramakrishnan and S. S. Mandal, Phys. Rev. B **62**, 6786 (2000).

[54] B. I. Halperin and David R. Nelson, J. Low Temp. Phys. **36**, 599 (1979).

[55] P. A. Lee and N. Nagaosa, Phys. Rev. B **45**, 966 (1992); ibid. **46**, 5621 (1992).

[56] P. W. Anderson, *Theory of Superconductivity in the High-T_c Cuprate Superconductors* (Princeton, NJ, 1997).

[57] J. Engelbrecht, M. Randeria and C. A. R. Sá de Melo, Phys. Rev. B **55**, 15153 (1997).

[58] J. Schmalian, S. Grabowski and K. H. Bennemann, Phys. Rev. B **56**, R509 (1997).

[59] A. V. Chubukov, Europhys. Lett. **44**, 655 (1998).

[60] A scheme for probing the energetic structure of pairing fluctuations in the pseudogap regime has recently been proposed and developed by Jankó and collaborators; see Refs. [24, 61].

[61] B. Jankó (unpublished, 1998) has extended the approach of Ref. [24] to the cases of pseudogap-pseudogap and normal-pseudogap tunneling.

[62] We shall assume that the adopted tunneling geometry minimizes cancellations in the tunneling amplitude due to the d-wave form of the pairing state. The phase we refer to is the overall phase of the order parameter.

[63] See, e.g., Refs. [64–66].

[64] A. F. Andreev, Zh. Eksp. Teor. Fiz **46**, 1823 (1964) [Sov. Phys. JETP **19**, 1228 (1964)].

[65] J. Demers and A. Griffin, Can. J. Phys. **49**, 285 (1970); A. Griffin and J. Demers, Phys. Rev. B **4**, 2202 (1971).

[66] G. E. Blonder, M. Tinkham and T. M. Klapwijk, Phys. Rev. B **25**, 4515 (1982).

[67] See, e.g, B. Z. Spivak and D. E. Khmel'nitskiĭ, Pis'ma Zh. Eksp. Teor. Fiz. **35**, 334 (1982) [JETP Lett. **35**, 412 (1982)].

[68] By *mesoscopic* we mean (linear) sizes comparable to or smaller than the dephasing length L_ϕ for single-particle motion. For contact sizes larger than $\min(L_\phi, \xi_\phi)$, the conductance is essentially given by the classical addition of parallel conductance at the scale $\min(L_\phi, \xi_\phi)$. As we are ultimately concerned with probing ξ_ϕ, we shall assume that $L_\phi > \xi_\phi$.

[69] F. W. J. Hekking and Yu. V. Nazarov, Phys. Rev. Lett. **71**, 1625 (1993).

[70] See, e.g., A. Dimoulas, J. P. Heida, B. J. v. Wees, T. M. Klapwijk, W. v. d. Graaf, and G. Borghs, Phys. Rev. Lett. **74**, 602 (1995); P. G. N. de Vegvar, T. A. Fulton, W. H. Mallison, and R. E. Miller, Phys. Rev. Lett. **73**, 1416 (1994); H. Pothier, S. Guéron, D. Esteve, and M. H. Devoret, Phys. Rev. Lett. **73**, 2488 (1994); H. Nakano and H. Takayanagi, Phys. Rev. B **47**, 7986 (1993); C. J. Lambert, J. Phys. Condens. Mat. **5**, 707 (1993).

[71] For a review of the tunneling formalism see, e.g., G. D. Mahan, *Many Particle Physics* (Plenum, New York, 1990), Sec. 9.3.

[72] As applied, e.g., by T. Tsuzuki, Prog. Theor. Phys. **41**, 1600 (1969).

[73] See, e.g., A. A. Abrikosov, L. P. Gorkov, and I. E. Dzyaloshinski, *Methods of Quantum Field Theory in Statistical Physics* (Dover, New York, 1975), Chap. 7.

[74] To treat the case of d-wave pairing, one would need to take into account directional anisotropy in the tunneling matrix element as well as in $\Delta_{\mathbf{k}}$. We expect that the results will be qualitatively the same for this case.

[75] We note that the assumptions leading to Eqs. (3.18) or (3.31) (i.e. $k_{\rm B}T \ll eV$ and $eV \ll \Delta$) imply that T must be chosen to be much smaller than Δ. Thus, we expect the experiment to be most feasible for strongly underdoped cuprates, in which $T_{\rm c}$ is small relative to Δ.

[76] J. M. Kosterlitz, J. Phys. C **7**, 1046 (1974).

[77] See, e.g., Ref. [14].

[78] The interplay between Andreev reflection and disorder on the normal side of an NS junction was already discussed in the literature some time ago; see B. J.

van Wees, P. de Vries, P. Magnée, and T. M. Klapwijk, Phys. Rev. Lett. **69**, 510 (1992) and Ref. [69] .

[79] For a pedagogical review of the effects of disorder in conductors, see, e.g., J. Rammer, *Quantum Transport Theory* (Perseus, Reading, MA, 1998).

[80] For the dephasing length in the normal metal contact to be long compared with the interface size we expect that the system will have to be at low temperatures. Higher temperatures will also smear the current-voltage signal [cf. the Fermi distribution in Eq. (3.14)] Thus, we expect that the experiment will necessarily involve strongly underdoped cuprate materials with a small T_c.

[81] See, e.g., A. I. Larkin and D. E. Khmel'nitskiĭ, Usp. Fiz. Nauk **136**, 533 (1982) [Sov. Phys. Usp. **25**, 185 (1982)]; G. Bergmann, Phys. Rep. **107**, 1 (1984); S. Chakravarty and A. Schmid, Phys. Rep. **140**, 193 (1986).

[82] J. Y. T. Wei, N.-C. Yeh, D. F. Garrigus and M. Strasik, Phys. Rev. Lett. **81**, 2542 (1998).

[83] D. P. Arovas, A. J. Berlinsky, C. Kallin and S.-C. Zhang, Phys. Rev. Lett. **79**, 2871 (1997).

[84] E. Demler, A. J. Berlinsky, C. Kallin, G. B. Arnold and M. R. Beasley, Phys. Rev. Lett. **80**, 2917 (1998).

[85] P. M. Goldbart and D. E. Sheehy, Phys. Rev. B **58**, 5731 (1998), see also Chap. 5.

[86] W. A. Little, Phys. Rev. **156**, 108 (1967).

[87] J. S. Langer and V. Ambegaokar, Phys. Rev. **164**, 498 (1967).

[88] P. W. Anderson and G. Toulouse, Phys. Rev. Lett. **38**, 508 (1977); G. E. Volovik, Pis'ma ZhETF **27**, 605 (1978) [JETP Lett. **27**, 573 (1978)].

[89] P. M. Goldbart and P. Ao, Phys. Rev. Lett. **64**, 910 (1990).

[90] D. E. Sheehy and P. M. Goldbart, Phys. Rev. B **57**, 8131 (1998).

[91] Note that the parameter that we call g is identical to the parameter called $\tilde{g}$ in Ref. [83].

[92] B. D. Josephson, Adv. Phys. **14**, 419 (1965).

[93] D. McCumber and B. I. Halperin, Phys. Rev. B **1**, 1054 (1969).

[94] Stability with respect to small variations has not been checked for the stationary antiferromagnetic hedgehog configuration with a superconducting core.

[95] For a table of homotopy groups see the *Encyclopedic Dictionary of Mathematics*, edited by Kiyosi Itô (MIT Press, Cambridge, MA, 1993), App. A, Table 6.VI.

[96] For pedagogical introductions to the topological theory of defects in condensed matter, see: N. D. Mermin, Rev. Mod. Phys. **51** 591 (1979); and M. Kléman, *Points, Lines, and Walls: in liquid crystals, magnetic systems, and various ordered media* (John Wiley, New York, 1983).

[97] For application of this machinery in the context of ^{3}He, see D. Bailin and A. Love, J. Phys. A: Math. Gen. **11**, 821 (1978); J. Phys. A: Math. Gen. **11**, L219 (1978). For a general discussion of homotopy theory, see N. Steenrod, *The Topology of Fibre Bundles* (Princeton University, Princeton, NJ, 1951).

[98] This means that the homomorphisms are not necessarily *onto* (i.e. do not map onto every element of the following group) and are not necessarily *one-to-one* (i.e. some elements of one group may be mapped into more than one element of the following group).

[99] P. E. Cladis and M. Kléman, J. Phys. (Paris) **33**, 591 (1972); R. B. Meyer, Phil. Mag. **27**, 405 (1973); for a discussion, see P. G. De Gennes and J. Prost, *The Physics of Liquid Crystals* (Oxford University Press, 1993), Sec. 4.3.1.

[100] We thank G. Volovik for bringing to our attention to related phenomena in superfluid ^{3}He.

[101] G. E. Volovik and V. P. Mineyev, Zh. Eksp. Teor. Fiz. Pis'ma Red. **24**, 605 (1976) [JETP Lett. **24**, 561 (1976)]. For a discussion of textures in ^{3}He, see Chap. 7 of D. Vollhardt and P. Wölfle, *Superfluid Phases of Helium-three* (Taylor and Francis, London, 1990), and references therein.

[102] I. F. Lyuksyutov, Zh. Eksp. Teor. Fiz. **75**, 358 (1976) [JETP **48** 178 (1978)].

[103] It may be interesting to consider the implications of phase-coherence between superconducting cores, although this may not be straightforward to produce.

[104] L. G. Aslamazov and A. I. Larkin, Phys. Lett. **26A**, 138 (1968); Fiz. Tverd. Tela **10**, 1104 (1968) [Sov. Phys. Solid St. **13**, 2474 (1972)]. For discussions, see I. O. Kulik and I. K. Yanson, *The Josephson Effect in Superconductive Tunneling Structures* (Israel Program for Scientific Translation, Jerusalem, 1972); M. Tinkham, *Introduction to Superconductivity* (McGraw-Hill, New York, 1975); Chap. 7; A. A. Abrikosov, *Fundamentals of the Theory of Metals* (North-Holland, 1988), Sec. 19.6.

[105] We thank Boris Altshuler for alerting us to the issue of charging effects.

[106] For a discussion, see Chap. 2 of the book by Tinkham cited in Ref. [104].

[107] D. Waxman and K. D. Ivanova-Moser, Ann. Phys. **226**, 271 (1993).

[108] We can always choose the Jacobian to be unity by an appropriate choice of parameters.

Vita

Daniel Edward Sheehy was born in St. Paul, Minnesota on April 19, 1973. He attended high school at the St. Paul Academy and Summit School, graduating in 1991. He received the Bachelor of Arts degree in physics from The Johns Hopkins University in 1995 and the M.S. degree in physics from the University of Illinois in 1998.